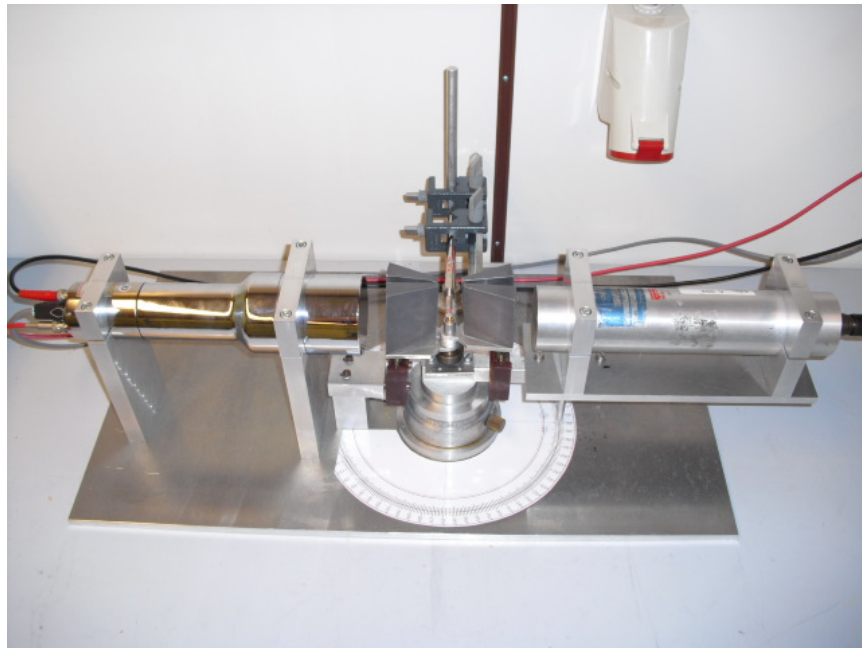


Advanced lab course for  
bachelor students in physics  
**RWTH Aachen**



**Experiment T3**  
 **$\gamma\gamma$ -Angular Correlation**

February 2023

# Contents

<b>1</b>	<b>Introduction</b>	<b>4</b>
<b>2</b>	<b>Theory</b>	<b>4</b>
2.1	$\gamma$ -Energy Spectroscopy with Scintillation Detectors . . . . .	4
2.2	Angular Distribution of $\gamma\gamma$ Events . . . . .	7
2.3	True and Random Coincidences . . . . .	8
2.4	Radioactive Sample: $^{22}\text{Na}$ . . . . .	9
2.5	Radioactive Sample: $^{60}\text{Co}$ . . . . .	10
<b>3</b>	<b>Employed Hardware</b>	<b>12</b>
3.1	Fast and Slow Coincidence Circuit . . . . .	12
3.2	NIM Standard and Delaying Signals . . . . .	13
3.3	Main Amplifier . . . . .	13
3.4	Single-Channel Analyser (SCA) . . . . .	14
3.5	Multichannel Analyser (MCA) . . . . .	14
3.6	Coincidence Unit . . . . .	15
3.7	Counter . . . . .	15
<b>4</b>	<b>Procedure</b>	<b>16</b>
4.1	Energy Spectroscopy . . . . .	16
4.2	Coincidence Measurement . . . . .	18
4.2.1	$^{22}\text{Na}$ Annihilation Peak . . . . .	18
4.2.2	Finding the Annihilation Peak . . . . .	21
4.2.3	Angular Distribution of $^{60}\text{Co}$ . . . . .	21
<b>5</b>	<b>Analysis</b>	<b>23</b>
5.1	Energy Spectroscopy . . . . .	23
5.2	Coincidence Measurement . . . . .	24
5.2.1	$^{22}\text{Na}$ Annihilation Peak . . . . .	24
5.2.2	Angular Distribution of $^{60}\text{Co}$ . . . . .	24
<b>A</b>	<b>Räumliche Gestalt der <math>\gamma</math>-Strahlung</b>	<b>26</b>
<b>B</b>	<b>Die Parität</b>	<b>29</b>

<b>C</b>	<b>Koinzidenzmessung</b>	<b>30</b>
<b>D</b>	<b>Introduction of the PicoScope</b>	<b>33</b>
D.1	Setup of the PicoScope . . . . .	33
D.1.1	Hardware . . . . .	33
D.1.2	Software . . . . .	33
D.2	Using the software . . . . .	34
D.2.1	General remarks . . . . .	34
D.2.2	<i>Scope Mode</i> and <i>Persistence Mode</i> . . . . .	34
D.2.3	Changing the display of the input signal . . . . .	36
D.2.4	Trigger . . . . .	37
D.2.5	Saving waveforms . . . . .	38
D.2.6	Measurements . . . . .	39
D.2.7	<i>Math Channel</i> . . . . .	40

# 1 Introduction

Nuclear spectroscopy is one of the most important fields of nuclear physics.  $\gamma$  quanta are emitted in transitions between excitation states of a nucleus. By measuring the angular distributions of these emissions, conclusions can be reached on nuclear properties like nuclear spin and parity.

Often, excited nuclei transition to the ground state via a decay cascade. In many cases, the lifetime of an intermediate state is so short, that the nucleus cannot change its orientation within this time. In this case, the first quantum can be used to fix the radiation axis. The direction of the second quantum is then measured relative to this. For  $\gamma\gamma$ -angular correlation, such correlated  $\gamma$  quanta or “coincidences” are detected. The angular distribution of the coincidence rate provides a window into the radiation characteristics of the nucleus.

## 2 Theory

### 2.1 $\gamma$ -Energy Spectroscopy with Scintillation Detectors

To detect the  $\gamma$  radiation, scintillation detectors with connected photomultipliers are used. The detection of the  $\gamma$  radiation happens indirectly via the interaction of the photons with the scintillator material. There are three significant effects that determine the characteristics of the energy spectrum of a sample and cause either complete or partial energy transfer of the photon to electrons.

- The photoelectric effect occurs when the photon interacts with an absorber atom. The photon is absorbed and passes its energy  $h \cdot \nu$  on to a previously bound electron, which is now free. The free electron has an energy equal to the energy of the photon minus its binding energy  $E_{electron} = h \cdot \nu - E_{binding}$ . The majority of the photon’s energy therefore remains as the kinetic energy of the electron. The unoccupied spot, which is left behind by the freed electron, is usually filled quickly by an electron from the outer shells of the atom, the higher-energy electrons again releasing their energy through photons, which are absorbed in the outer shells and are therefore rarely detected. The photoelectric effect is especially dominant for absorber materials with high nuclear charge numbers  $Z$ . For the cross section  $\sigma$ , we can write  $\sigma \propto \frac{Z^5}{E_\gamma^3} \cdot [1]$
- The Compton effect involves an interaction of the photon with an electron from the absorber material. The photon changes direction and transfers part of its energy to the electron. The energy transfer depends on the impact angle between the photon and the electron and ranges from zero to almost  $h \cdot \nu$ . The remaining photon energy is

$$h \cdot \nu' = \frac{h \cdot \nu}{1 + (1 - \cos(\theta)) \cdot \frac{h \cdot \nu}{m_e \cdot c^2}},$$

so the distance of the Compton edge ( $\theta = 180^\circ$ ) from the photopeak in the energy spectrum is

$$E_C = \frac{h \cdot \nu}{1 + 2 \cdot \frac{h \cdot \nu}{m_e \cdot c^2}}.$$

Assuming  $h \cdot \nu \ll \frac{1}{2} \cdot m_e \cdot c^2$ , it follows that  $E_C \approx \frac{1}{2} \cdot m_e \cdot c^2$ . Up until the Compton edge, there is a continuous spectrum, which corresponds to Compton scattering for angles from  $0^\circ$  to  $180^\circ$ . The energy spectrum also contains energies between the Compton edge and the photopeak. These can be explained by multiple Compton scattering. The cross section of Compton scattering is given by the Klein-Nishina formula. The backscattering peak is also due to Compton scattering. It is caused by photons that interact with the materials surrounding the detector and scatter by more than  $120^\circ$ . The backscattering peak is located around  $E_{backscattering} = E_C \approx \frac{1}{2} m_e c^2$ . [1]

- The third interaction is pair creation. If the photon energy  $E_\gamma = h \cdot \nu$  is larger than twice the rest energy of an electron  $m_e c^2$ , then pair creation is possible, producing an electron and a positron from the photon. Additional photon energy becomes kinetic energy of the created electron-positron pair, which both lose it again via interactions. The kinetic energies satisfy  $E_{electron}^{kin} + E_{positron}^{kin} = h \cdot \nu - 2 \cdot m_e \cdot c^2$ . The produced electron stays in the absorber material, the positron annihilates with another electron in its vicinity. This produces two photons of energy 511 keV. If both of the annihilation photons and the photons due to the deposition of kinetic energy are registered, this once again adds up to the energy of the photon and so this case is registered in the spectrum as part of the photopeak. If one of the annihilation photons escapes from the material without being detected, this creates a single-escape peak at  $E_{single-escape} = h\nu - m_e c^2$ . If both annihilation photons escape, the resulting double-escape peak lies at  $E_{double-escape} = h\nu - 2m_e c^2$ .

In addition to these three effects, there are many other effects and superpositions of effects, which lead to a continuous spectrum. For certain spectra, this leads to an observable and measurable linear background, which is why in the analysis of the spectra the peaks are determined using a superposition of Gaussian curves and a first-degree polynomial.

All three interactions described also cause the attenuation of  $\gamma$  radiation in matter. The linear attenuation coefficient  $\mu$  can be calculated using the sum of the interaction cross sections. The intensity of the photons decreases exponentially and is described by  $I = I_0 \cdot e^{-\mu x}$  after penetrating the absorber material by the distance  $x$ .

The scintillator material should fulfil certain requirements. First, the material used should be sensitive to the type of radiation and the relevant energy range. Secondly, it should result in a relation between photon energy and scintillation photons that is as linear as possible, which later results in a linear relation between photon energy and pulse height of the voltage pulse. The scintillator material should also be transparent to the produced scintillation photons. It should be malleable and have a refractive index of ca. 1,5, to ensure an efficient transition to the photocathode of the photomultiplier. The scintillators employed here use thallium-doped sodium iodide (NaI(Tl)). This is an inorganic scintillator material. Inorganic materials are slower than organic materials, but offer a large and linear light yield. NaI(Tl) is linear on almost the entire energy range and because of this a standard material for scintillation detectors today. The disadvantages of NaI(Tl) are its mechanical strength (fragile) and the fact that it is hygroscopic and as such must be protected from moisture in the air.

The processes inside the scintillator material can be explained using the energy band model. In inorganic materials, the conduction band contains free electrons, whereas the valence band contains bound electrons. In a pure material, there are no allowed states within the band gap between both bands. By doping with an activator, however, the new excited states and ground states of the activator are added. If a charged particle moves through the material,

electron-hole pairs are created. The created holes move towards activator atoms and ionise these, exciting them to higher energy levels. The electrons, on the other hand, are put into the conduction band and move freely through the crystal, until they reach ionised, excited activator atoms. The neutralised activator atom quickly returns to the ground state, emitting a scintillation photon in the wavelength range of visible light.

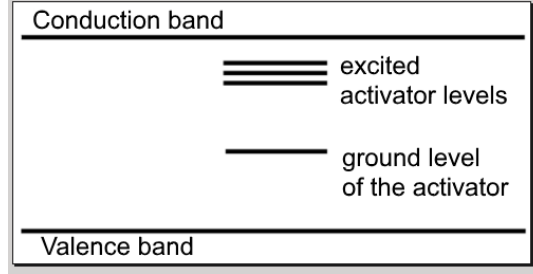


Figure 1: Band model of a scintillator material with valence and conduction bands of the base material and additional levels of the introduced activator material.

Because the scintillator is transparent to light in the visible spectrum, the created scintillation photons reach the photocathode of the photomultiplier (PM). Here, they create one electron in the PM through the external photoelectric effect. These electrons are bundled and then accelerated by an applied voltage onto multiple, successive dynodes. The electrons are always accelerated so strongly, that they create secondary electrons at each dynode. For average dynode materials, roughly 5 to 10 electrons are produced per dynode and incident electron. The amplification can be described by  $V = \delta^N$ , where  $N$  is the number of dynodes, the PM used in this experiment has 10, and  $\delta$  is the number of freed secondary electrons. The creation of secondary electrons is a statistical process, so the uncertainty is  $\sqrt{\delta}$ . In this way, several hundred incident photons can be converted into a measurable voltage pulse. Typically,  $10^5 - 10^7$  electrons reach the anode for each electron freed from the photocathode, depending on the PM.

Important quantities for the characterisation of the detectors used are the energy resolution and the efficiency. The energy resolution dictates, which photon energies can still be measured separately and the efficiency indicates, how many of the arriving photons are converted into a measured signal. The energy resolution is energy-dependent. The relation can be described by

$$\frac{\Delta E}{E} = \sqrt{a^2 + \frac{b^2}{E}} \quad (1)$$

A distinction is made between two types of detector efficiency. The total efficiency is defined as  $\epsilon_{tot} = \frac{\text{registered events}}{\text{events emitted by the source}}$  and the intrinsic efficiency as  $\epsilon_{int} = \frac{\text{registered events}}{\text{events reaching the detector}}$ . In our case, the intrinsic efficiency is of interest, i.e. the amount of events reaching the detector that are converted into an electrical signal. The following holds:

$$\epsilon_{int} = \frac{4 \cdot \pi \cdot r^2 \cdot m}{F_D \cdot A \cdot I_\gamma}$$

The registered events are calculated from the count rate  $m$ , i.e. the sum of all registered particles averaged over the measurement time. The events reaching the detector can be

calculated from the the number of particles produced by the decay considered and a geometrical factor. The number of considered particles corresponds to the product of the activity of the sample A and the fractional contribution of the considered decay to the total activity, described by  $I_\gamma$ . The geometrical factor approximately results from the fraction of the surface area of a sphere of radius r, which is the distance between the source and the detector, covered by the detector surface  $F_D$ . This approximation assumes that the particles propagate uniformly in all directions and that the curvature of the sphere at the detector surface can be neglected. *Additional information on energy spectroscopy and the workings of the detectors can be found in the instructions to experiments T1 and T2.*

## 2.2 Angular Distribution of $\gamma\gamma$ Events

Two different  $\gamma\gamma$  production mechanisms are investigated during this experiment. The first is the production of  $\gamma\gamma$  by  $e^+e^-$  annihilation. This produces two  $\gamma$ 's at an angle of  $180^\circ$ . The second mechanism is the creation by a decay cascade inside a nucleus. For such a decay with a transition from  $I_i$  to  $I_f$ , the distribution of emitted  $\gamma$ 's is isotropic, if

- all  $(2 \cdot I_i + 1)$  possible substates with different magnetic quantum numbers ( $m$ ) are occupied equally and
- all possible transitions from  $(I_i, m_i)$  to  $(I_f, m_f)$  are observed.

For the simple transition from  $I_i = 1$  to  $I_f = 0$ , for example, there are three possibilities with probabilities:

$$W^+ = \frac{3}{16} \cdot \pi \cdot (1 + \cos^2\theta) \quad (2)$$

$$W^0 = \frac{3}{8} \cdot \pi \cdot \sin^2\theta \quad (3)$$

$$W^- = \frac{3}{16} \cdot \pi \cdot (1 + \cos^2\theta) \quad (4)$$

Due to the limited energy resolution of the employed detectors, only the combination of these transitions can be observed and so one gets:

$$W = \sum W_i = \frac{3}{4} \cdot \pi \quad (5)$$

So the intensity is distributed isotropically across all angles  $\theta$ . Only when the magnetic substates are occupied unevenly, i.e. distributed anisotropically, is it possible to measure an angular distribution.

The coincident measurement offers a solution to this problem. Because one can only measure the angular distribution relative to a fixed quantisation axis, the emission of the first  $\gamma$ -quantum fixes such an axis. The substates of the intermediate system are occupied unevenly with respect to this direction: the result is an angular distribution of the second quantum  $W(\theta)$ . If the lifetime of the intermediate state is very short, then the second  $\gamma$  can be measured within a defined time window. Such an event is called a **coincidence**.

A general angular distribution or „angular correlation“  $W(\theta)$  can be written as:

$$W(\theta) = 1 + A_2 \cdot P_2(\cos\theta) + A_4 \cdot P_4(\cos\theta) + \dots + A_{2k_{max}} \cdot P_{2k_{max}}(\cos\theta) \quad (6)$$

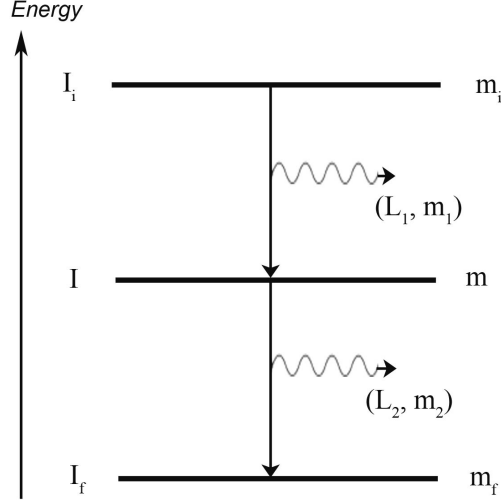


Figure 2: Quantum numbers for a  $\gamma\gamma$  cascade.

, where

$$k_{max} = \min(I, L_1, L_2) \quad (7)$$

The angular momentum quantum numbers of the first and second  $\gamma$  quantum are here called  $L_1$  and  $L_2$ . The initial, intermediate and final states have nuclear spin quantum numbers  $I_i$ ,  $I$  and  $I_f$  (see fig. 2).  $P_\nu(\cos\theta)$  denote the Legendre polynomials.

*For a detailed derivation, have a look at the appendix (currently German-only). The appendix is not part of the pre-experimental discussion.*

### 2.3 True and Random Coincidences

A distinction is made between true coincidences, from which conclusions on physical reactions can be drawn, and random coincidences, which are caused by background events, noise or similar processes. If one assigns two events individual detection probabilities  $p_1$  and  $p_2$ , then the single count rates of both events are  $N_1 = p_1 \cdot A$  and  $N_2 = p_2 \cdot A$ , provided both events are emitted by the same source with activity  $A$ . The true coincidence count rate, i.e. the count rate for the simultaneous occurrence of both events, therefore is  $N_{true}^{coinc} = p_1 \cdot p_2 \cdot A$ . The measured coincidence count rate  $N_{measured}^{coinc}$ , however also contains a contribution from the count rate of random coincidences  $N_{rand}^{coinc}$ . The following is true:

$$N_{measured}^{coinc} = N_{true}^{coinc} + N_{rand}^{coinc} \quad (8)$$

When considering the random coincidences, the resolution time is of importance, since the count rate  $N_{rand}^{coinc}$  indicates, how many events occur within the resolution time independent of physical reactions. The resolution time of the measurement process is determined by the pulse width, the rise time of the pulse and the response times of the devices used. If one

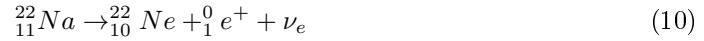
assumes the idealised case where both events need the same time  $\tau$ , then the resolution time is  $T_A = 2\tau$ . This results in [8]

$$N_{rand}^{coinc} = T_A \cdot N_1 \cdot N_2 = 2\tau \cdot p_1 \cdot p_2 \cdot A^2 \quad (9)$$

The resolution time should be chosen such that all true coincidences are recorded, but simultaneously as few as possible random coincidences occur. It is thus necessary to determine the optimal resolution time (see section 4.2).

## 2.4 Radioactive Sample: $^{22}\text{Na}$

First, we consider the longest-lived artificial isotope of sodium,  $^{22}\text{Na}$ , which has a half-life of 2,60 years[8]. The isotope is converted via  $\beta^+$  decay (by emission of a positron) to neon:



The emitted positrons annihilate with electrons of the sodium itself or with electrons of the setup (see fig. 3).

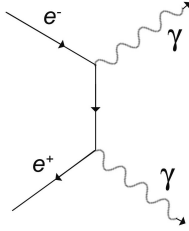


Figure 3:  $e^-e^+$  annihilation.

Two photons are produced in this process, which fly away from each other at an angle of  $180^\circ$  due to momentum conservation. For exactly this reason, the isotope is very useful for the coincidence measurement. The ideal angular distribution is of the form  $W(\theta) = \delta(\theta - \pi)$ , which can be compared to measurements by the coincidence setup. From this, the operability of the setup can be tested and at the same time, a systematic error on the angle measurement can be estimated, e.g. a zero offset due to shifted collimators.

The most important transitions are shown in fig. 4. The most probable transition is the  $0,5459\text{MeV}$   $\beta^+$  transition:

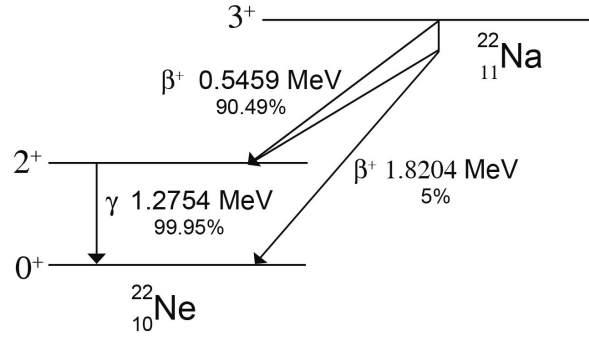


Figure 4: Simplified decay scheme of  $^{22}\text{Na}$  with transition energies and probabilities.

## 2.5 Radioactive Sample: $^{60}\text{Co}$

$^{60}\text{Co}$  is especially well-suited for  $\gamma\gamma$  angular correlation, partly due to its very clear decay scheme with a relatively unambiguous decay mode (fig. 5). The isotope is first converted to nickel via a  $\beta^-$  decay:



after which the nucleus is in one of two possible excited states. 99.88% of the time, the nucleus occupies the higher excited state and can emit two  $\gamma$  quanta via the intermediate state. In the rarer case, the nucleus occupies the intermediate state and emits just one  $\gamma$  quantum. After the emission of the  $\gamma$  quanta, the nucleus is once again in the ground state. The lifetime of the  $2^+$  – intermediate state is only 0,7 ps, so in the case of the most common decay mode, the emission of the second  $\gamma$  quantum is well-measurable as a coincidence [9].

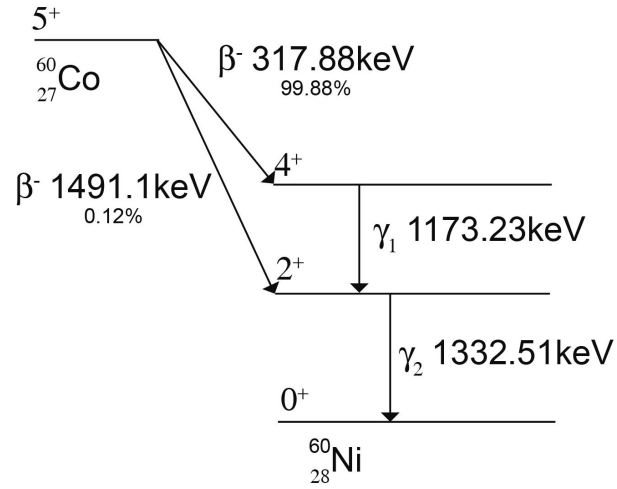


Figure 5: Simplified decay scheme of  $^{60}\text{Co}$  with transition energies and probabilities.

As can be seen in the decay scheme, this is a  $4(2) - 2(2) - 0$  cascade. Using table 4 on page 32 and equation (6), the following correlation function is expected to be found by a coincidence measurement:

$$W(\theta) = 1 + \frac{1}{8} \cdot \cos^2(\theta) + \frac{1}{24} \cdot \cos^4(\theta) \quad (12)$$

Higher powers of  $\cos(\theta)$  do not contribute to the correlation function, due to the additional constraint in equation (6). The following is true for this decay cascade:

$$k_{max} = \min(I, L_1, L_2) = 2 \quad (13)$$

Using table 3 on page 30, one can see that both transitions are due to electromagnetic quadrupole radiation.

### 3 Employed Hardware

#### 3.1 Fast and Slow Coincidence Circuit

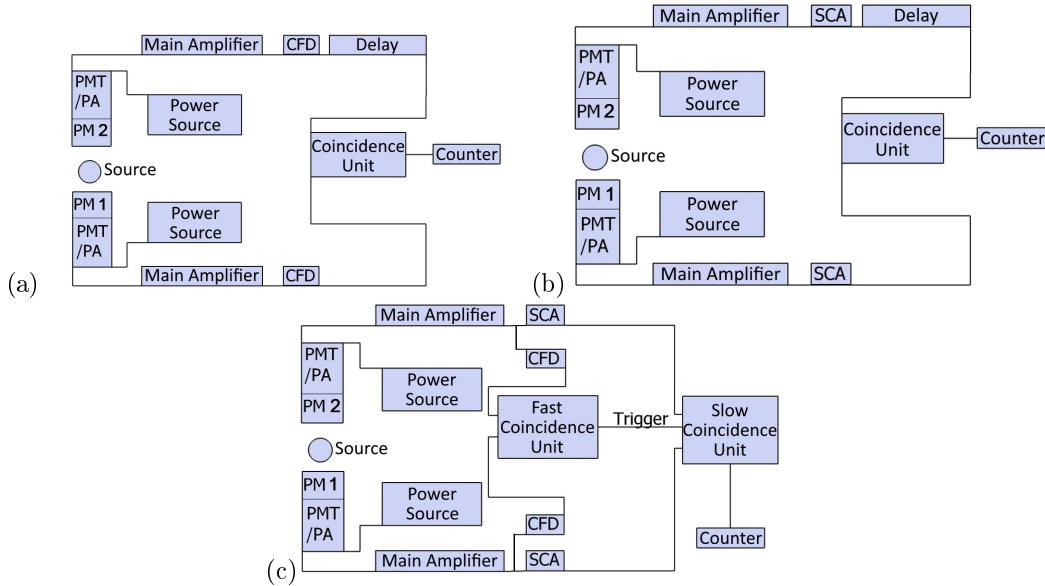


Figure 6: Circuit principles of (a) fast coincidence circuit with CFD and time-sorting of the signals (b) slow coincidence circuit with SCA and sorting of signals by pulse height (c) combined fast-slow coincidence circuit, where the slow circuit with SCA is triggered by the fast circuit.

A distinction is made in measurement engineering between three coincidence methods, which satisfy different requirements. The fast coincidence has a good time resolution, the slow coincidence a good energy resolution and the fast-slow coincidence is a combination of both methods. The first part of the setups of all three methods is the detector. In this case, it detects the photons and generates a voltage pulse, which height is proportional to the energy of the detected photons.

For the fast coincidence method, the photomultiplier signal is amplified and then passed on to a constant fraction discriminator (CFD). The CFD records exact timestamps and emits logic pulses. The logic signals from both CFDs are then combined in a coincidence unit, which emits a signal only if both signals arrive within the set resolution time. Depending on the electronics used, one of the branches processes the signal faster than the other, which must be taken into account and corrected using a delay unit. The signals from the coincidence unit can then be registered using e.g. a counter.

For a slow coincidence, the signal is put into a single-channel analyser (SCA) after passing through the main amplifier. Here, the pulses are filtered by their pulse height, which is proportional to the received photon energy, emitting a logic pulse only when a pulse height lies within a chosen range. The signals from the SCAs are then also combined into a coincidence unit after passing through a delay circuit and analysed with a counter.

The resolution time of the fast coincidence circuit is significantly shorter (about 4 ns) than the resolution time of the slow coincidence circuit (about 500 ns). This is used in the combined fast-slow coincidence method, where the fast coincidence circuit is used to trigger the slow one.

### 3.2 NIM Standard and Delaying Signals

One standard for physical dimensions and electrical units in nuclear and particle physics is based on individual building blocks, the nuclear instrument modules (NIMs). This standard defines the external dimensions of electrical modules. The basic principle is that every module fits in every mount. Because of this, connectors for power supplies are also standardised. The voltage is provided via the frame, the NIM crate. All modules described here follow the NIM standard.

To connect two modules, coaxial cables are used. These consist of a cylindrical capacitor with a dielectric. The cables used delay the signal by around 5,14 ns/m. This property is used in delay units, in which cables of different lengths can be combined as desired using switches. Connecting delay units in series can be done without problems, though it should be noted that each connection between units introduces a delay corresponding to its length and that each delay module has an intrinsic delay of 2,5 ns. In most cases, especially in a coincidence circuit, the time difference between two signals is relevant. A time difference can be evened out by sending the earlier signal through a longer cable or delay units.

### 3.3 Main Amplifier

The same type of main amplifier is used for both detectors. Depending on the setup, this is either a separate module or it is combined with the SCA. This module allows for the amplification of the signal using a coarse and a fine setting (course and fine gain). The separate modules also offer the option of pulse shaping. The amplifier settings are chosen, such that all channels of the pulse height analyser are used by the energy range considered. For the pulse height analysers used, this means that the voltage pulses should lie between 0 V and 10 V to be recorded. The signals from the preamplifier integrated into the PM lie in the mV range, so the proper amplification factors lie around 500. Since the signal strengths of the PMs and their respective preamplifiers are slightly different, the amplification factors of the main amplifiers also differ between the branches. The amplification factor is the product of the fine gain and the coarse gain. It should also be noted, that the preamplifiers output signals with a positive polarity. The polarity should be set accordingly for the main amplifiers.

Adjustable signal shaping serves to improve the signal-to-noise ratio. A bell curve is used for the signal. The shaping time corresponds geometrically to the standard deviation and is therefore a measure of the pulse width. The shaping time should be picked, such that there is sufficient time to collect all charge from the detector, while simultaneously being short enough to enable high count rates. The longer the shaping time, the better the signal-to-noise ratio. However, if the shaping time is chosen too long, multiple separate events can be combined into one at high count rates. Commonly used shaping times for modern photomultipliers range from 0,5  $\mu$ s to 2  $\mu$ s.

The separate main amplifiers provide two outputs, one with a unipolar and one with a bipolar signal, whereas the integrated main amplifiers only have a unipolar one. The advantage of

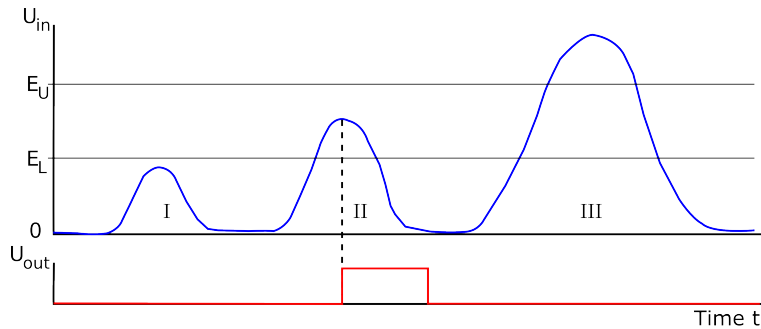


Figure 7: Sketch of the behaviour of the single-channel analyser. The first (I) pulse in the input voltage (blue line)  $U_{in}$  lies below the set minimum height of  $E_L$ . This limit is the lower level  $E$  adjusted on the module. The second (II) pulse lies within the set window between  $E_L$  and  $E_U$ , where  $E_U$  is  $E + \Delta E$  as set on the module. This pulse (II) produces a square logic pulse of fixed duration in the output signal  $U_{out}$ . This output pulse is created, when the maximum of the pulse is detected. Neither of the other pulses (I + III) satisfy the criteria (too small or too large) and therefore do not generate an output pulse.

the bipolar signal is that the position of the zero crossing is independent of the amplitude and therefore well-suited as a time signal. However, the bipolar signal also has more noise than the unipolar signal. For spectroscopy and the coincidence measurement, the unipolar signal is used.

### 3.4 Single-Channel Analyser (SCA)

Depending on the setup, two different modules are used as single-channel analysers: either a separate module or combined with the amplifier. Nonetheless, both function in the same way and differ only in some details.

The defining job of an SCA is to filter signals according to their amplitude. If the amplitude of an input pulse lies within the set limits, a digital, square output pulse is created. If the pulse height lies outside of the set limits, no output pulse is generated. On the modules employed, the lower limit  $E$  and the window width  $\Delta E$  can be set. The upper limit is  $E + \Delta E$ . The lower limit as well as the window width can be picked from the range 0 V to 10 V on both SCA modules. On the separate SCA module, the window range can additionally be switched from 10 V to 1 V, allowing for a finer adjustment of small window widths.

### 3.5 Multichannel Analyser (MCA)

For energy spectroscopy, it is counted how many times which energy is measured within a predefined time. To this end, the amplified pulse height, which is linear in the detected scintillation light, which in turn is linear in the energy of the absorbed  $\gamma$ , is measured and digitised. In digitisation, the pulse heights in the range 0 – 10 V are converted to an integer number from 0 to 16383. Each of these integers corresponds to a channel with its own counter. All channels are of equal width. During the analysis, each channel can be assigned not only to a voltage range, but also to an energy range via calibration.

The MCA employed (Multiport II) is read out and controlled by the software "Gammamessung und -analyse". This software allows for the adjustment of several settings, i.a. measurement times and the number of channels used. To achieve a better energy resolution, it makes sense to set the number of channels to the highest possible value of 16384.

The software offers many more possibilities, like e.g. an automatic energy-channel calibration, which is, however, not used. The data of the software can be saved as ASCII files (.TKA), in which the first two lines indicate the specified and actual measurement time. Each following line corresponds to a channel.

### 3.6 Coincidence Unit

The job of the coincidence unit is to generate a logic pulse when two or more signals arrive within a predefined time window, the resolution time. The opposite is anticoincidence, where no pulse is generated if two signals coincide within the resolution time. The coincidence module used can switch between two time scales. It supports the ranges 10 ns to 100 ns and 0,1  $\mu$ s to 1  $\mu$ s. Please note that the adjustment via the wheel is not linear. Because of this, you should definitely take a look at page 4-3 of the respective Canberra manual (Model 2040 Coincidence Analyzer), which is provided in this lab course's room.

### 3.7 Counter

A counter is to be connected to the coincidence unit to count the logic pulses. The module used additionally has a clock, meaning a measurement time can be set. The counter has two channels which can be counted in parallel. The tallies are shown on a display. Resetting is done using a button, as are starting and stopping the measurement. Using the clock, a maximum measurement time can be set as wished in units of 0,01 seconds or 0,01 minutes. It should be noted that the time is entered in the form  $NM \cdot 10^p$ . This means that  $N$  indicates the 10's,  $M$  the 1's and  $p$  the power of 10 of the chosen time unit. Setting  $N$  and  $M$  to 0 turns off the clock.

## 4 Procedure

Before you insert any sources into the setup, you should perform the following mechanical adjustments and measurements:

- Using the callipers, measure the distance between the detectors and the source.
- Adjust the aperture of the lead wedges (collimator) in front of the detector, such that the distance between the inner sides is roughly 0,5 cm on the side near the detector. Loosen the four set screws slightly from below in order to do this.
- Try to align both collimators as symmetrically around the radiation axis and perpendicularly to the detector surface as possible.
- Measure the distance from the detectors to their respective collimator.
- Set up an angle of  $0^\circ$  between the detectors.
- A photo from perpendicularly above is helpful during any potential troubleshooting later on.

### 4.1 Energy Spectroscopy

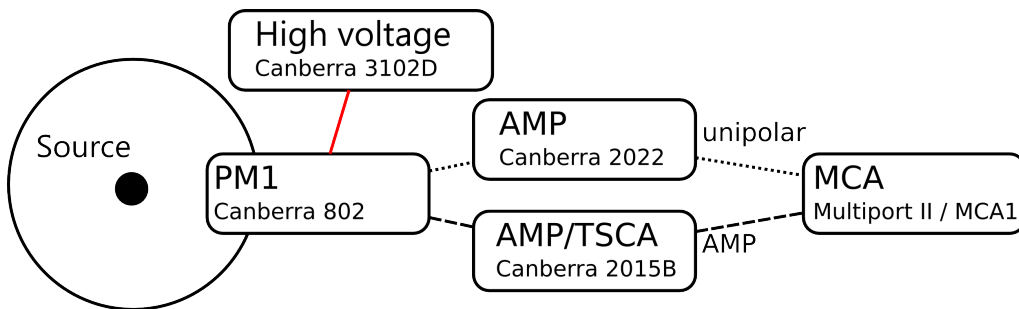


Figure 8: Setup for energy spectroscopy. Depending on the setup, either the dashed or the dotted signal path is used.

- Supply PM1, which is mounted in a fixed position, with a high voltage of 490 V (left *Canberra 3102D* module, HV supply, cables have already been connected, please do not remove them). Please note the format of the numbers on the HV power supply: the smallest number shown corresponds to 10 V, i.e. the required 490 V correspond to 0,49 on the display.
- The signal cable of PM1 is already connected to the input of an amplifier. Make sure that the polarity is set to +. Connect the unipolar output to the first input of the MCA. If signal shaping is adjustable, choose a shaping time of  $0,5 \mu\text{s}$ .
- Start the read-out software (desktop icon "Gammamessung und -analyse") on the PC (user Praktikum, no password). Place the  $^{152}\text{Eu}$  sample in front/on top of the

detector and click on *Start* inside the program to start the measurement. Choose the amplification settings, such that the entire spectrum is recorded. For this, you will have to wait around 30 seconds before all peaks are discernible. Hint: *3 small peaks should be visible on the left and a fourth peak on the far right!* The amplification settings you chose should be on the order of ( $\approx 500$ ).

- Record the spectra of  $^{152}\text{Eu}$ ,  $^{60}\text{Co}$  and  $^{22}\text{Na}$  for 10 minutes each and save each of the spectra as a *.TKA*-file. This creates an ASCII file with the measured data. In the created file, the first line indicates the specified measurement time and the second line the actual measurement time in seconds. Each of the following lines corresponds to one of the MCA's channels. Additionally perform a blank measurement in order to be able to estimate potential background effects. Use the same, unaltered amplifier settings for all isotopes.
- At home, you should determine the energy resolution and efficiency of the detector from these measurements. Think about which other quantities you have to determine to do this and write these down. Use the data recording time to acquaint yourself with the different modules using the second detector (same settings as PM1) and the oscilloscope. For example, take a look at the differences between a unipolar and a bipolar signal, check how the signal changes when the shaping time is changed and look at the combination of the amplified signal (using a T connector if needed) and the SCA output. Hint: *use the Single Seq. button on the oscilloscope if necessary.*

## 4.2 Coincidence Measurement

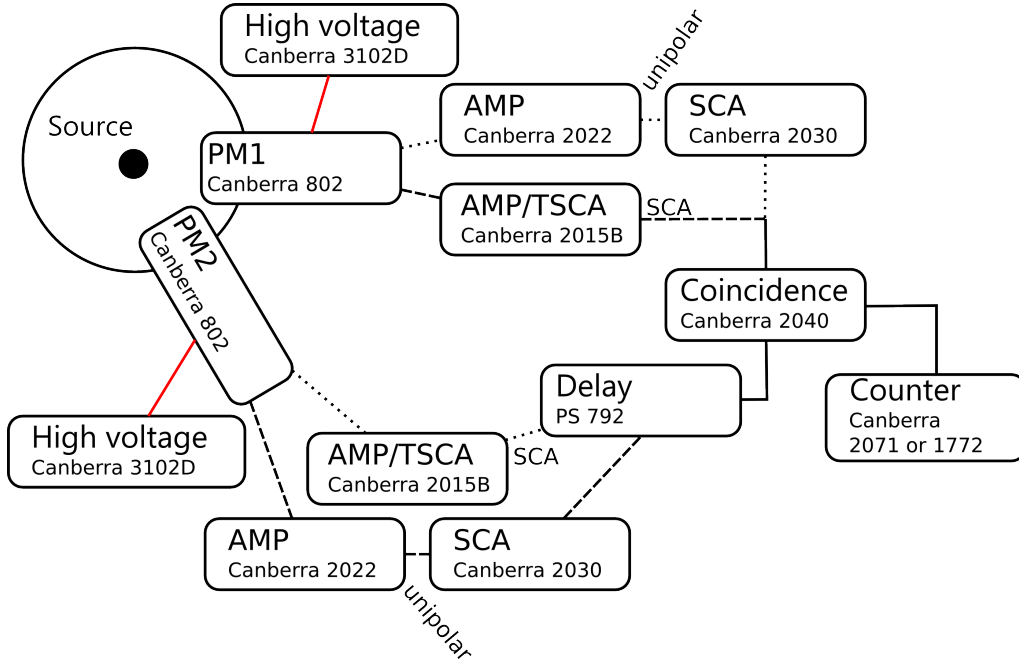


Figure 9: The setup used for the coincidence measurement. Depending on the setup, either the dashed or the dotted signal path is used.

### 4.2.1 $^{22}\text{Na}$ Annihilation Peak

- Supply  $PM2$  with a high voltage of 490 V (right *Canberra 3102D* module, HV supply, cables have already been connected, please do not remove them). The signal cable of  $PM2$  is already connected to the input of the second main amplifier (right module). Set the polarity to positive and, if possible, set the shaping time to  $0,5 \mu\text{s}$ . Place the  $^{60}\text{Co}$  or  $^{152}\text{Eu}$  source in front of the detector and, as before, choose a good amplifier setting ( $\approx 500$ ) for  $PM2$ 's signal branch by using the MCA.
- Now place the  $^{22}\text{Na}$  source on top/in front of the detector. If needed, connect the unipolar outputs of the amplifiers with the inputs of the respective SCAs mounted to the right. Next, connect the output of one of the SCAs with the input of the counter. Adjust a fixed window setting  $\Delta E$  of 0,2 V and scan the entire spectrum. To do this, vary the *lower level*  $E$  in steps of 0,20 V across the range 0 – 10 V and find out at which voltage the annihilation peak can be found for both detectors. Using this data, choose a value for the lower level  $E$  for which, for a window width  $\Delta E$  of approximately 0,8 V, the entire peak of the spectrum is recorded.
- Now determine the resolution time and the setup's optimal delay. Place the  $^{22}\text{Na}$  sample in between both detectors. First, adjust the resolution time of the coincidence module to roughly 30 ns. Connect one SCA output with the input of the delay module. Then connect the output of the first delay stage to the second delay stage of the delay

module. Finally, connect the output of the second delay stage as well as the output of the second SCA module to the coincidence module. The output of the coincidence module should be connected to the counter. Both channels used should be switched to “IN” on the coincidence module. Now scan the delays in steps of 30 ns and record the corresponding counter readings after a fixed measurement time of e.g. 10 s. Note that even without any additional delay switched on, each delay stage has an intrinsic delay of 2,5 ns. After going through all delays for one PM, connect both SCA outputs directly to the coincidence unit. This measurement corresponds to a delay of 0 ns. After that, delay the other PM. If you plot the counted events against the delay, the result is approximately a Gaussian. Adjust the delay to the mean of this distribution. Next, vary the resolution time in sensible steps (not necessarily equidistant) up to the maximum possible value of the longer range and, again, for each setting count the events within a sensible period. Plot the event counts against the true resolution time and determine an optimal resolution time setting. In case you cannot identify an optimal resolution time from this graph, choose a resolution time equal to the width of the Gaussian distribution of the delay fit. For the conversion of the set resolution time to a true time, please see page 4-3 of the Canberra manual.

- The signal of one SCA should now pass through the delay unit and be connected to an input of the coincidence module. The signal of the second SCA should be connected directly to another input of the coincidence unit.
- Count the events from  $-10^\circ$  to  $10^\circ$  in steps of  $2^\circ$  with both detectors in coincidence for a measurement time of 2 minutes each.

The PicoScope can be used to make the preamplified analog signal of the PM, the unipolar output from the amplifier module and the digital signal of the SCA visible. The following setup could be established

1. PM output  $\rightarrow$  amplifier input (back side)
2. PM output (back side recommended)  $\rightarrow$  PicoScope
3. Unipolar amplifier output (back side recommended)  $\rightarrow$  PicoScope
4. Unipolar amplifier output  $\rightarrow$  SCA input
5. SCA output (back side recommended)  $\rightarrow$  PicoScope

It is recommended to use one side (e.g. the backside) of the modules for connections with the PicoScope to keep the wiring well-arranged. Note that a  $50 \Omega$  termination resistance behind the SCA is required. One experimental setup has SCA and amplifier combined in one module. The output is shown in Figure 10. In order to find amplified signal and the corresponding output, a simple edge trigger is useful (cf. Sec. D.2.4). Possible values for the input range etc. of the channels and the trigger can be found in the figure or alternatively in Table ?? (Some values differ from the ones in the figure especially for the pre-amplifier as another PMT is used there). To see both outputs, it is strongly recommended to trigger on the SCA output. If a trigger is applied on the amplified signal, one often sees no SCA signal because it has only an output in a small energy window. But in case there is an SCA signal, a peak from the amplifier is always expected so it is best to trigger on the SCA output. A

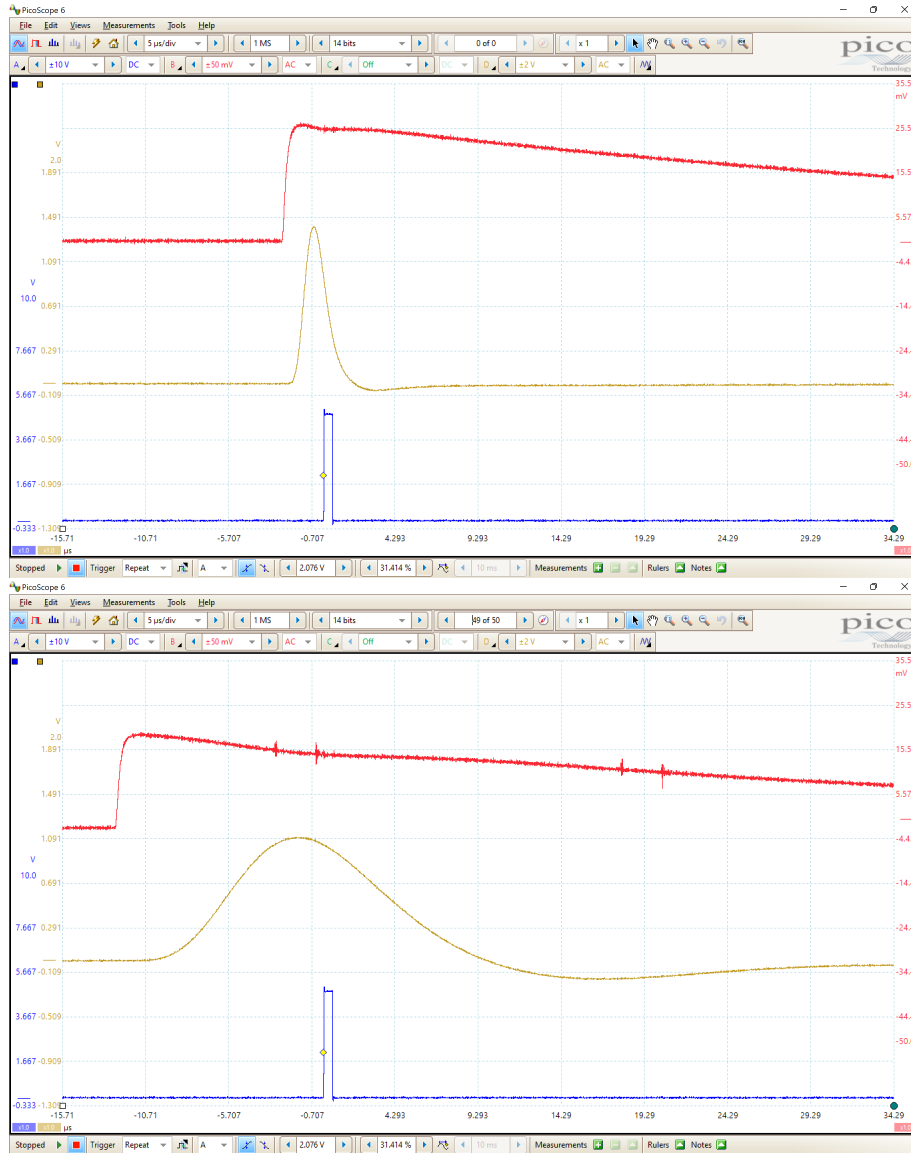


Figure 10: The preamplified PM signal (red, channel B) and the corresponding amplifier (yellow, channel D) and SCA output (blue, channel A). A trigger was applied to find the relative short signals. Note that the input ranges of the signals are different and the signals are vertically shifted by a scale offset. The upper image corresponds to a shaping time of  $0.5 \mu\text{s}$  and the lower has  $4 \mu\text{s}$ . Amplifier and SCA are calibrated to the  $\gamma$  peak of  $\text{Na}^{22}$ .

scale offset (cf. Sec. D.2.3) can be used to shift the signals vertically.

The SCA output should always have an amplitude of about 5 V and a pulse width of about 500 ns. When changing the lower energy level  $E$  of the SCA, the SCA amplitude and pulse width do not change but the amplitude of the amplifier output increases or decreases when an SCA signal is observed and if  $E$  was increased or decreased, respectively. The energy window  $\Delta E$  controls the upper energy level of the SCA. If  $\Delta E$  is large, the amplitudes of multiple amplifier outputs for the corresponding SCA signal vary more in comparison to a narrow energy window.

The effect of different shaping times becomes visible. A short shaping time gives a short amplifier peak which becomes visible after the PM output reaches its maximum after a relatively short period of time. A longer shaping time gives a broader and more delayed amplifier peak.

#### 4.2.2 Finding the Annihilation Peak

The measurement feature of the PicoScope can be used to count rising edges automatically. Heretofore, the counting is performed with a counter module but using the PicoScope has the advantage of being able to read out the data automatically and store it for further processing. One SCA output is connected to the PicoScope preferably with a  $50\ \Omega$  termination resistor. At the SCA,  $\Delta E = 0.2\ \text{V}$  is set and  $E$  is set to the lower (or upper) end of the interval which is of interest. In general, a full sweep of the 10 V range of the SCA has to be performed but due to the use of the MCA beforehand one often has a rough estimate in which voltage range the  $\gamma$ -peak is. In this experiment, the *Collection Time* should be as large as possible while still being able to perform the measurement. In order to achieve this, the *Number of Samples*, (cf. D.2.6) of the PicoScope must be decreased, the resolution should be small and not used channels should be deactivated. The sample interval must be small enough to capture the SCA peaks. Possible values for the settings and the measurement are shown in Table 1. The *Input range*, *Offset* and *Resolution* are not important as digital HIGH signals are considered. The *Collection Time* and measurement time should be as large as possible to obtain good statistics but they are usually limited by the measurement. Reducing one or the other value might be necessary to perform a successful measurement. A measurement is shown in Figure 11.

#### 4.2.3 Angular Distribution of $^{60}\text{Co}$

- Proceed similarly to the  $^{22}\text{Na}$  measurement. Set a fixed window setting (window  $\Delta E$ ) of 0,2 V and scan the spectrum. To this end, vary the *lower level*  $E$  in steps of 0,20 V across 0 – 10 V and find out at which voltages the two peaks can be found. Based on these result, set the SCAs to one photopeak each with a window width of 0,80 V.
- Connect all cables in the same way as for the last step of the measurement of the  $^{22}\text{Na}$  annihilation peak. Keep the previously determined optimal delay and resolution time values.
- Measure the angular distribution of  $^{60}\text{Co}$  from  $0^\circ$  up to the maximum possible angle ( $\approx -82^\circ$ ) in steps of  $10^\circ$ . Perform one test measurement for a timespan of 5 minutes

Table 1: Proposed settings for counting peaks received from the SCA. If the measurement cannot be performed (i.e. - - are displayed in the measurement section), some settings should be decreased. Always make sure that the *Number of Samples* is large enough for capturing the SCA peaks.

Settings	Values
Input range	$\pm 5$ V
Collection time	10 ms/div
Offset	not necessary
Resolution	8 bits
Sample interval (depends on Number of Samples)	$2^* < 500$ ns
$2^*$ Number of Samples	$\geq 300$ kS (for a Collection Time of 10 $\mu$ s/div)
	Measurement
Mode	Rising or Falling Edge Count
$2^*$ Span	Whole Trace (or between rulers with appropriate time span if measurement is not successful)
Threshold	Automatic

at 0°. Based on the theoretical expectation, the test measurement and the expected statistical errors, determine a suitable measurement duration for each angle.

- Finally, delay one *PM* maximally. Measure one more time for the determined measurement duration and subtract the measured number from the previous results. What is measured for these settings and why do you subtract the measurements from each other?

Before the SCA signals are fed into the coincidence module, a delay module is interconnected and adjusted such that a maximum of coinciding signals is found. The problem arises that the event rates are comparably low ( $\mathcal{O}(1$  Hz) or lower) and thus relatively long *Collection Times* of the PicoScope are needed to count a sufficient number of signals. The procedure to measure count rates with the PicoScope is presented in the following.

The instructions for the measurement of the rate of coincidence signals cannot only be applied in the part of the experiment where an optimal delay has to be found but for all measurements with the coincidence module.

Two setups of the measurement are deemed to be possible. Either a moderate *Collection Time* and many waveforms are captured or a long *Collection Time* is used and only one waveform is considered. The first measurement can be used if the count rate is not too low. If so, the sample standard deviation (calculated by the PicoScope software) can be used as an uncertainty estimate but if the number of counts per sample is  $\mathcal{O}(1)$  the sample standard deviation is usually similar or larger than the mean number of counts. The second option is to use a long *Collection Time* where the uncertainty estimate is given by the square root of the counts. This is the same procedure as using a counter module.

In either case, some settings should be applied always in order to enable a successful measurement. It must be ensured that the *Slow Sampling Mode* is not activated (cf. Sec. D.2.6). The *Hardware Resolution* (8 bits) and the *Number of Samples* should be as small as possible.

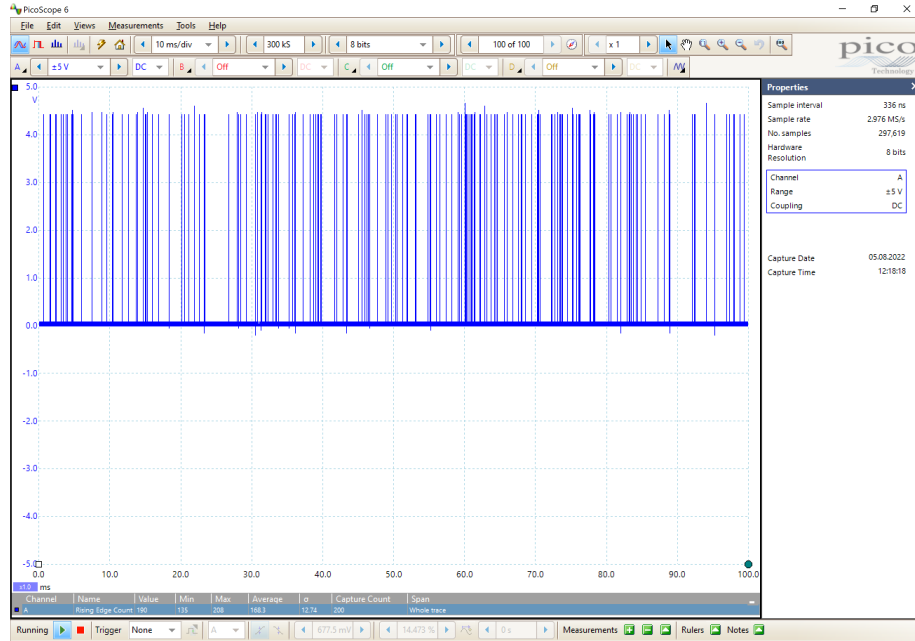


Figure 11: Using the PicoScope to determine the SCA count rates. The *Properties* window (right) is used to monitor the sample interval. The presented count rate is comparably high for this experiment.

The latter must be large enough to resolve the coincidence signals ( $\approx 1 \mu\text{s}$ ) and the *Collection Time* should not be larger than necessary.

For the delay measurement, the settings can be as in Table 2. These settings can also be applied in other coincidence measurements, e.g. in the measurement of the angular distribution of  $\gamma\gamma$  events.

## 5 Analysis

### 5.1 Energy Spectroscopy

1. Plot the spectra of  $^{152}\text{Eu}$ ,  $^{60}\text{Co}$  and  $^{22}\text{Na}$ . In each case, identify the position of the photopeak and, if possible, the Compton edge.
2. Create a calibration line between the photon energy and the channel number. To this end, determine the position of the photopeaks by fitting a Gaussian with a linear background.
3. Determine the energy resolution of the scintillator as a function of energy by determining the full width at half maximum of the photopeaks. Determine the coefficients  $a$  and  $b$  defined in equation (1).
4. Determine the efficiency  $\varepsilon$  of the detector from the measured rates of the photopeaks. For this, calculate the activity of the samples used on the day of the experiment.

Table 2: Proposed settings for counting peaks of the coincidence module for the determination of the optimal delay. If the measurement cannot be performed (i.e. - - are displayed in the measurement section), some settings should be decreased. Always make sure that the *Number of Samples* is large enough for capturing the coincidence peaks. These settings could also be used for other counting measurements in the experiment with the coincidence module.

Settings	Values
Input range	$\pm 10$ V
Collection time	5 s/div
Offset	-1 V or less
Resolution	8 bits
Sample interval (depends on Number of Samples)	$2^* < 1 \mu s$
2*Number of Samples	$\geq 100$ MS (for a Collection Time of 5 s/div)
	Measurement
Mode	Rising or Falling Edge Count
2*Span	Whole Trace (or between rulers with appropriate time span if measurement is not successful)
Threshold	Automatic

## 5.2 Coincidence Measurement

### 5.2.1 $^{22}Na$ Annihilation Peak

1. Plot the counted events against the delay time and against the resolution time. From these plots, determine the resolution time and the optimal delay of the setup.
2. Plot the count rates of the coincidence measurement against the angle  $\theta$  and fit a Gaussian curve to the data. What is the mean of the distribution? How large is the standard deviation? To what extent does this correspond to the theoretical expectation (see section 2.4)? From now on, assume the standard deviation of the Gaussian to be the statistical error of the angular measurement. If necessary, correct the angles by a systematic deviation.

### 5.2.2 Angular Distribution of $^{60}Co$

1. Plot the correlation function  $W(\theta)$  for the measured angular range, where:

$$W(\theta) = N_{measured}^{coinc}(\theta) / N_{measured}^{coinc}(0^\circ) \cdot W_{theo}(0^\circ) \quad (14)$$

2. Now perform a fit of the form

$$W(\theta) = 1 + a_2 \cdot \cos^2(\theta) + a_4 \cdot \cos^4(\theta) + \dots \quad (15)$$

to the measured angular range. Up to which power of  $\cos(\theta)$  should be included in the fit and why? Confirm the theoretical values of the coefficients  $a_i$ , as well as the goodness of your fit (error analysis!).

## References

- [1] Glenn F. Knoll: *Radiation Detection and Measurement*. John Wiley & Sons, New York, 1979.
- [2] Haro v. Buttler: *Einführung in die Grundlagen der Kernphysik*, Akademische Verlagsgesellschaft, Frankfurt am Main, 1964.
- [3] T. Mayer-Kuckuk: *Physik der Atomkerne*, Teubner Studienbücher, Stuttgart, 1994.
- [4] Jackson, *Classical Electrodynamics*, J. Wiley and Sons.
- [5] W.N. Cottingham & D.A. Greenwood: *An Introduction to Nuclear Physics*, Cambridge University Press.
- [6] M.J. Martin & P.H. Blichert-Toft: *Radioactive Atoms*, Nuclear Data Project, Oak Ridge, Tennessee, 1970.
- [7] Erwin Bodenstedt: *Experimente der Kernphysik und ihre Deutung*, B.I. Wissenschaftsverlag
- [8] H.U. Schmidt: *Meßelektronik in der Kernphysik*, B.G. Teubner, Stuttgart, 1986.
- [9] M.J. Martin & P.H. Blichert-Toft: *Radioactive Atoms*, Nuclear Data Project, Oak Ridge, Tennessee, 1970.

## A Räumliche Gestalt der $\gamma$ -Strahlung

Bei der  $\gamma\gamma$ -Winkelkorrelation interessieren wir uns ausschließlich für die  $\gamma$ -Emission, die als elektromagnetische Strahlung wahrgenommen wird.

Um die räumliche Gestalt der Strahlungsintensität zu verstehen, kann man die Maxwellgleichungen im Vakuum verwenden:

$$\operatorname{rot}\vec{E} = -\frac{\partial\vec{B}}{\partial t}; \quad \operatorname{rot}\vec{B} = \frac{1}{c^2} \frac{\partial\vec{E}}{\partial t}; \quad (16)$$

Es wird dabei berücksichtigt, dass die Felder quellenfrei sind:

$$\operatorname{div}\vec{E} = \operatorname{div}\vec{B} = 0 \quad (17)$$

Mit der Annahme, dass die  $\vec{E}$ - und  $\vec{B}$ -Felder eine Zeitabhängigkeit der Form  $e^{-i\omega t}$  besitzen und mit der nichtrelativistischen Dispersionsrelation  $c = \frac{\omega}{k}$ , bekommt man:

$$\operatorname{rot}\vec{E} = ick\vec{B}; \quad \operatorname{rot}\vec{B} = -\frac{ik}{c}\vec{E} \quad (18)$$

Die Gleichungen können nun ineinander eingesetzt werden, um die bekannte Wellengleichungen zu bekommen:

$$(\Delta + k^2)\vec{E} = 0; \quad (\Delta + k^2)\vec{B} = 0 \quad (19)$$

Wir suchen zunächst die Lösungen der entsprechenden skalaren Wellengleichung:

$$(\Delta + k^2)\psi(\vec{r}) = 0 \quad (20)$$

Um eine Quelle gehen die Strahlung kugelförmig aus. Es wird deswegen der kugelförmige Ansatz gewählt:

$$\psi(r, \theta, \phi) = \frac{U(r)}{r} \cdot P(\cos\theta) \cdot Q(\phi) \quad (21)$$

Durch Aufstellung von Differentialgleichungen in Kugelkoordinaten und Verwendung eines Potenzreihenansatzes (siehe z.B. [2]) bekommt man als Lösungen der  $\theta$ -Abhängigkeit die zugeordnete Legendrepolynome:

$$P_l^m(x) = \frac{(-1)^m}{2^l l!} (1 - \cos^2\theta)^{m/2} \frac{d^{l+m}}{d(\cos\theta)^{l+m}} (\cos^2\theta - 1)^l, \quad (22)$$

wobei  $l = 0, 1, 2, 3, \dots$  und  $m = 0, \pm 1, \pm 2, \dots \pm l$  sind. Die Felder sind also quantisiert. Die  $\varphi$ -abhängigen Lösungen sind ganz einfach durch

$$Q(\varphi) = e^{im\varphi} \quad (23)$$

gegeben. Die Radialabhängigkeit wird durch die sphärischen Besselfunktionen beschrieben:

$$j_L(kr) = \sqrt{\frac{\pi}{2kr}} J_{l+\frac{1}{2}}(kr), \quad (24)$$

wobei  $J_{l+\frac{1}{2}}$  die gewöhnlichen Besselfunktionen sind. Für unsere Zwecke ist diese radiale Abhängigkeit aber nicht interessant, da wir später nur Winkelverteilungen betrachten werden. Die  $\varphi$ - und  $\theta$ -Terme der Lösungen können wir aber als Kugelflächenfunktionen zusammenfassen:

$$Y_{lm}(\theta, \varphi) = \sqrt{\frac{2l+1}{4\pi} \frac{(l-m)!}{(l+m)!}} \cdot P_l^m(\cos\theta) \cdot e^{im\varphi} \quad (25)$$

Die Anregungszustände des Kerns können als Eigenfunktionen des Kernspins  $\vec{I}$  beschrieben werden. Beim Übergang zwischen Anregungszuständen werden  $\gamma$ -Quants mit Energien emittiert, die den Energiedifferenzen der Zustände entsprechen. Deshalb ist es auch logisch, dass das Strahlungsfeld der Kerne auch als Eigenfunktionen des Drehimpulses  $\vec{l}$  beschreiben werden kann. Im nächsten Schritt suchen wir die Lösungen der Feldgleichungen (19), indem wir den Drehimpulsoperator

$$\vec{l} = -i(\vec{r} \times \vec{\nabla}) \quad (26)$$

an die skalaren Wellenfunktion  $\psi(\vec{r})$  anwenden. Wir bekommen mit Hilfe der vektoriellen Kugelflächenfunktion  $X_l^m(\theta, \varphi) = \frac{1}{\sqrt{l(l+1)}} \vec{l} \cdot Y_l^m(\theta, \varphi)$  folgende Abhängigkeiten:

$$E_l^m \propto X_l^m; \quad \text{und} \quad B_l^m \propto -\frac{i}{kc} \text{rot} \left( E_l^m \right) \quad (27)$$

$$B_l^m \propto X_l^m; \quad \text{und} \quad E_l^m \propto \frac{ic}{k} \text{rot} \left( B_l^m \right) \quad (28)$$

Durch Summieren dieser Lösungen für alle möglichen  $m$  und  $l$  bekommt man eine vollständige Multipolentwicklung des elektromagnetischen Strahlungsfeldes. Wir bezeichnen nun der Kernspin des Anfangs- bzw. Endzustands durch  $\vec{I}_1$  bzw.  $\vec{I}_2$ . Wegen der Drehimpulserhaltung bekommt man folgenden Auswahlregeln für die Quantenzahlen:

$$|I_1 - I_2| \leq l \leq I_1 + I_2; \quad \text{mit} \quad m = m_1 - m_2 \quad \text{und} \quad |m| \leq l, \quad (29)$$

wobei meistens die niedrigste Multipolordnung dominiert. Für eine Erklärung dazu wird auf [3] hingewiesen.

In der Kernspektroskopie ist es wichtig zwischen elektrischer  $E$  und magnetischer  $M$  Multipolstrahlung zu unterscheiden. Leider ist es nur durch die Messung der Polarisation der  $\gamma$ -Strahlung möglich, den Strahlungscharakter, also ob es sich um eine  $El$ - oder  $Ml$ -Strahlung handelt, zu bestimmen. Es lässt sich aber theoretisch zeigen, dass die Übergangswahrscheinlichkeit für elektrische Multipolstrahlung viel höher als die für magnetische Multipolstrahlung bei derselben Ordnung ist.

Photonen werden in der Form eines  $2^l$ -Pol Multipolfelds der Multipolordnung  $l$  emittiert. Man merke, dass  $\hbar l$  dem vom Photon angenommenen Gesamtdrehimpuls entspricht, mit einer Projektion auf der  $z$ -Achse von  $m\hbar$ . Da das Photon einen intrinsischen Spin von 1 besitzt, ist der Wert  $l = 0$  nicht möglich. Abbildung 12 zeigt ein Beispiel von erlaubten und nicht erlaubten Übergängen anhand einer  $0 \rightarrow 1 \rightarrow 0$  Kaskade.

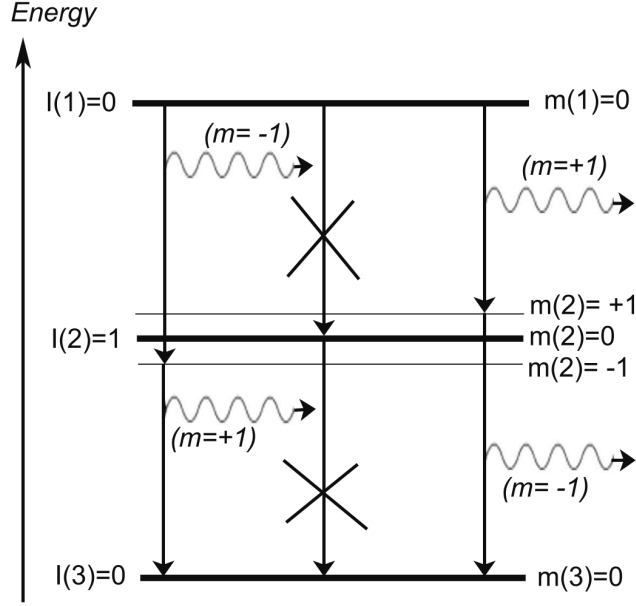


Figure 12: Beispiel erlaubter Übergänge für  $0 \rightarrow 1 \rightarrow 0$  Kaskade

Das Bild zeigt, dass für  $\Delta l = 1$  die Übergänge mit  $m = 0$  nicht erlaubt sind. Die physikalische Begründung dafür wird im folgenden Abschnitt diskutiert.

Letztendlich interessieren wir uns für die gemessene Intensität, die durch den Betrag des Poynting Vektors gegeben ist:

$$I = |\vec{S}| = \varepsilon_0 c E^2 \propto |X_l^m|^2 \quad (30)$$

Durch Anwendung Vernichtungs- und Erzeugungsoperatoren berechnet man für den Betrag der vektoriellen Kugelflächenfunktion [4]:

$$|X_l^m(\theta)|^2 = \frac{1}{2l(l+1)} [(l(l+1) - m(m+1)) \cdot |Y_l^{m+1}(\cos\theta)|^2 + (l(l+1) - m(m-1)) \cdot |Y_l^{m-1}(\cos\theta)|^2] \quad (31)$$

Durch Einsetzen von  $l = 1$  und  $m = 0, \pm 1$  bekommt man dann folgende Lösungen:

$$|X_1^0|^2 = \frac{3}{8\pi} \cdot \sin^2\theta; \quad \text{und} \quad |X_1^{\pm 1}|^2 = \frac{3}{16\pi} \cdot (1 + \cos^2\theta) \quad (32)$$

In Abbildung 13 werden die beide Lösungen als Polardiagramme dargestellt.

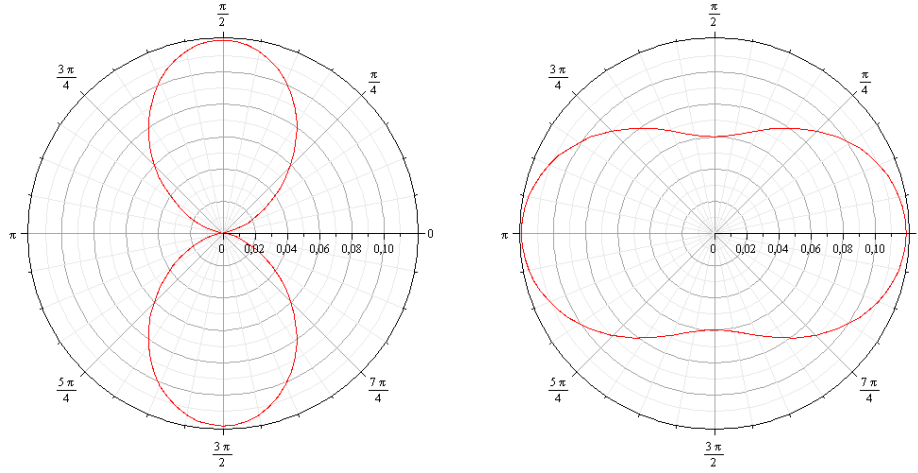


Figure 13: Gestalt der vektoriellen Kugelflächenfunktionen. Links:  $|X_1^0(\theta)|^2$  Rechts:  $|X_1^{\pm 1}(\theta)|^2$

Anhand dieser Bilder ist deutlich zu sehen, dass die Winkelverteilungen und deswegen auch die Intensitäten spiegelsymmetrisch zur  $90^\circ$ -Achse sind. Eine genauere Betrachtung der Gestalt der Kugelflächenfunktion, bzw. des zugeordneten Legendrepolynomes zeigt, dass beim Quadrieren nur gerade Potenzen von  $\cos(\theta)$  vorkommen. Es ist auch leicht zu sehen, dass die  $\varphi$ -abhängige Komponente  $Q(\varphi) = e^{im\varphi}$  beim Bilden des Betragsquadrats weg fällt. Deswegen ist die Winkelverteilung auch nur von  $\theta$  abhängig.

Für unsere in Abb. (12) gezeigten Beispiel mit  $\Delta I = 1$  sind  $|X_1^0(\theta)|^2$  und  $|X_1^{\pm 1}(\theta)|^2$  die beiden möglichen Winkelverteilungen. Wie man in Abb. (13) sieht, emittiert nur  $|X_1^{\pm 1}(\theta)|^2$  Quanten in  $z$ -Richtung. Die Winkelverteilung lässt sich aber nur gegen eine festgelegte  $z$ -Achse bestimmen. Es können also mit Hinsicht auf diese Quantisierungsrichtung nur die Zustände mit den magnetischen Quantenzahlen  $m = \pm 1$  besetzt werden.

## B Die Parität

Die Parität  $\Pi$  ist eine multiplikative Quantenzahl, die den Symmetriecharakter der Wellenfunktion bei Raumpiegelung beschreibt. Durch Spiegelung der Koordinatensystems an der Ursprung:

$$\vec{r} \rightarrow -\vec{r} \quad (33)$$

sollen sich bei Erhaltung der Parität die Eigenschaften des Systems nicht ändern. Die Wellenfunktion darf sich nur um den konstanten Wert  $\Pi$  ändern, wobei eine Rücktransformation wieder die ursprüngliche Funktion liefert, also  $\Pi^2 = 1$ . Ein System hat die Parität  $+1$  wenn gilt [5]:

$$\psi(-\vec{r}) = \psi(\vec{r}) \quad (34)$$

und hat die Parität  $-1$  für:

$$\psi(-\vec{r}) = -\psi(\vec{r}). \quad (35)$$

Die Parität ist in der elektromagnetischen Wechselwirkung eine Erhaltungsgröße des Systems. Durch Anwenden des Paritätsoperators auf die Multipolfelder, bekommt man für die elektrische Multipolstrahlung eine Parität von  $\Pi = (-1)^l$  und für die magnetische Multipolstrahlung eine Parität von  $\Pi = (-1)^{l+1}$ . Beim Übergang zwischen Kernzuständen 1 und 2 gilt also die Beziehung:

$$\Pi_1 = (-1)^l \cdot \Pi_2 \quad (36)$$

für elektrische Strahlung und

$$\Pi_1 = (-1)^{l+1} \cdot \Pi_2 \quad (37)$$

für magnetische Strahlung.

Anhand die beide Gleichungen ist es also grundsätzlich möglich zu bestimmen, ob beim Strahlungsübergang eine **Paritätsänderung** stattgefunden hat. In Tabelle (3) sind mehrere Beispiele von  $\gamma$ -Übergängen für unterschiedliche Multipolordnungen und Kernspinänderungen gegeben. Die in Klammern gesetzte M-Strahlungen sind wegen der niedrigen Übergangswahrscheinlichkeit praktisch nicht zu sehen.

Kernspinänderung $ \Delta I $	0	1	2	3	4
Paritätsänderung	E1; (M2)	E1; (M2)	M2; E3	E3; (M4)	M4; E5
keine Paritätsänderung	M1; E2	M1; E2	E2; (M3)	M3; E4	E4; (M5)

Table 3: Multipolordnung  $El$  und  $Ml$  in Abhängigkeit von der Kernspin- und Paritätsänderung. Entnommen aus [3].

Hinweis: Der Bezeichnung  $I^+$  bzw.  $I^-$  bedeutet Kernspin  $I$  mit Parität  $\Pi = \pm 1$ .

## C Koinzidenzmessung

Wie schon erwähnt wurde, ist die Intensität der emittierten Strahlung durch  $I \propto |X_l^m(\theta)|^2$  gegeben. Falls die magnetischen Unterniveaus  $m$  gleichwahrscheinlich besetzt sind, ist die emittierte Strahlung aber letztendlich eine Überlagerung aller verschiedenen Unterniveaus. Zum Beispiel gibt es für  $l = 1$  drei mögliche Unterniveaus:  $m = 0, +1, -1$ . Damit erhalten wir als Überlagerung:

$$I \propto |\vec{X}_1^0(\theta)|^2 + |\vec{X}_1^{+1}(\theta)|^2 + |\vec{X}_1^{-1}(\theta)|^2 = \frac{3}{8\pi} \sin^2\theta + \frac{3}{8\pi} (1 + \cos^2\theta) = \frac{3}{4\pi} \quad (38)$$

Die Intensität ist also isotrop über den ganzen Winkel  $\theta$ . Erst bei einer Ungleichbesetzung der magnetischen Unterzustände, also eine anisotrope Verteilung, ist es möglich, eine Winkelverteilung zu messen.

Die Koinzidenzmessung bietet eine Lösung zu diesem Problem. Es kann letztendlich nur mit Bezug auf eine feste Quantisierungsachse die Winkelverteilung gemessen werden. Durch Emission des ersten  $\gamma$ -Quants wird eine solche Achse festgelegt. Die Unterzustände des Zwischensystems hinsichtlich dieser Richtung sind dann verschieden besetzt: Man bekommt also eine Winkelverteilung für das zweite Quant  $W(\theta)$ . Wie in die Einführung schon erwähnt wurde, interessieren wir uns bei der  $\gamma\gamma$ -Winkelkorrelation für Zwischenzustände mit extrem

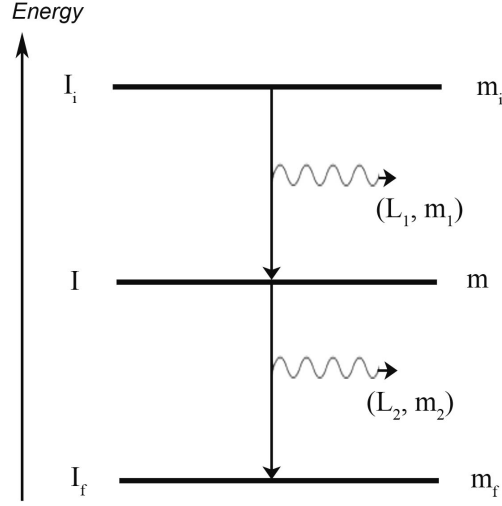


Figure 14: Quantenzahlen für  $\gamma\gamma$ -Kaskade mit reinen Multipolaritäten

kurzen Lebensdauer, so dass beide emittierten Photonen „praktisch zeitgleich“ ankommen (Lebensdauer des Zwischenzustands bis zu  $\sim ms$ ). Ein solches Ereignis wird **Koinzidenz** genannt.

Im Allgemeinen lässt sich die Winkelverteilung oder „Winkelkorrelation“  $W(\theta)$  in der Form [6]:

$$W(\theta) = 1 + A_2 \cdot P_2(\cos\theta) + A_4 \cdot P_4(\cos\theta) + \dots + A_{2k_{max}} \cdot P_{2k_{max}}(\cos\theta) \quad (39)$$

schreiben, mit

$$k_{max} = \text{Min}(I, L_1, L_2) \quad (40)$$

Hier werden die Drehimpuls Quantenzahlen des ersten und zweiten  $\gamma$ -Quants mit  $L_1$  und  $L_2$  bezeichnet. Die Anfangs-, Zwischen- und Endzustände haben die Kernspin Quantenzahlen:  $I_i$ ,  $I$  und  $I_f$  (siehe Abb. 14).  $P_\nu(\cos\theta)$  bezeichnen die Legendre Polynome.

Wie oben schon erwähnt wurde, betrachtet man in der Praxis meistens nur Übergänge mit reinen Multipolaritäten. Unter dieser Voraussetzung kann man eine Vereinfachung der Theorie, anders gesagt, eine „Naive Theorie“ verwenden. Wir betrachten nun wieder die Übergangswahrscheinlichkeit eines 2-Niveau-Systems und erhalten:

$$W(I_i, m_i \rightarrow I_f, m_f) = \text{konst.} \cdot G(m_i, m_f) \quad (41)$$

Hier ist der konstante Term durch das Kernmatrixelement gegeben. Der geometrische Term  $G$  ist gleich dem Quadrat des Clebsch-Gordan-Koeffizienten:

$$G(m_i, m_f) = \langle I_f l m_f M | I_i m_i \rangle^2, \quad (42)$$

wobei die Multipolarität der Strahlung wieder mit  $l$  und mit Projektor  $M = m_f - m_i$  bezeichnet wird. Für die Winkelverteilung der emittierten Gamma-Strahlung einer orientierten

Quelle erhält man [7]:

$$X_l(\theta) = \sum_{m_i, m_f} P(m_i) \cdot \langle I_f l m_f M | I_i m_i \rangle^2 \cdot |\vec{X}_l^{m_i - m_f}(\theta)|, \quad (43)$$

wobei  $|\vec{X}_l^{m_i - m_f}(\theta)|$  wieder die vektoriellen Kugelflächefunktionen sind. Wie schon erwähnt wurde, führt die Emission einer isotropen Quelle in eine festgelegte Richtung ( $z$ -Achse) zu einer Orientierung im Endzustand, was eine anisotrope Winkelverteilung der zweiten Strahlung zur Folge hat.

Wir betrachten deswegen wieder das Drei-Niveau-System, welches in Abb. 14 zu sehen ist. Wegen der Annahme reiner Multipolaritäten gilt  $m_2 = m - m_f$  und  $m_1 = m - m_i$ . Für die Besetzungswahrscheinlichkeit im mittleren Zustand  $I$ ,  $m$  bekommen wir:

$$P(m) = \sum_{m_i} \langle I L_1 m m_1 | I_i m_i \rangle^2 \cdot |\vec{X}_{L_1}^{m_i - m}(\theta = 0)| \quad (44)$$

Dies setzen wir in die Gleichung (43) für den zweiten Strahlungsübergang ein und erhalten für die Winkelkorrelationsfunktion:

$$W(\theta) = \sum_{m_f, m, m_i} \langle I L_1 m m_1 | I_i m_i \rangle^2 \cdot |\vec{X}_{L_1}^{m_i - m}(\theta = 0)| \cdot \langle I_f L_2 m_f m_2 | I m \rangle^2 \cdot |\vec{X}_{L_1}^{m - m_f}(\theta)| \quad (45)$$

Die Winkelverteilung lässt sich aber noch weiter simplifizieren. In der Fachliteratur wird die Korrelationsfunktion oft als Summe gerade Potenzen von  $\cos\theta$  dargestellt [2]:

$$W(\theta) = 1 + a_2 \cdot \cos^2\theta + a_4 \cdot \cos^4\theta + \dots + a_{2k_{max}} \cdot \cos^{2k_{max}}\theta, \quad (46)$$

wobei die Reihe wieder bei  $k_{max} = \min(I, L_1, L_2)$  abbricht. Es wurde auch das erste Glied auf 1 normiert, so dass man sich in der Praxis meistens nur für die Koeffizienten  $a_2$  und  $a_4$  interessiert. Sie können experimentell aus einer gemessenen Winkelverteilung bestimmt werden. Es werden in Tabelle 4 die theoretischen Zahlenwerte für  $a_2$  und  $a_4$  für einige  $\gamma$ -Kaskaden angegeben.

Kaskade $I_i(L_1) I(L_2) I_f$	$a_2$	$a_4$
0(1) 1(1) 0	+1	0
1(1) 1(1) 0	$-\frac{1}{3}$	0
1(2) 1(1) 0	$-\frac{1}{3}$	0
2(1) 1(1) 0	$-\frac{1}{5}$	0
3(2) 1(1) 0	$-\frac{3}{29}$	0
0(2) 2(2) 0	-3	+4
1(1) 2(2) 0	$-\frac{1}{3}$	0
2(1) 2(2) 0	$+\frac{2}{7}$	0
2(2) 2(2) 0	$-\frac{15}{13}$	$+\frac{16}{13}$
3(1) 2(2) 0	$-\frac{3}{29}$	0
4(2) 2(2) 0	$+\frac{1}{8}$	$+\frac{1}{24}$

Table 4: Die Koeffizienten  $a_2$  und  $a_4$  für einige  $\gamma$ -Kaskaden, entnommen aus [2].

Anhand dieser Tabelle werden die Begrenzungen der  $\gamma\gamma$ -Winkelkorrelation als Messmethode direkt klar. Die gemessene Winkelverteilung liefert keine eindeutige Zuordnung der Koeffizienten zu einer bestimmten Kaskade. Außerdem liefert diese Methode keine eindeutigen Informationen über die Parität des Zustands, da die obigen Ergebnisse sowohl für elektrische als auch magnetische Strahlung gelten. Information über die Parität kann nur über ein schon zum Teil bekanntes Bild des Zerfallsschemas gewonnen werden.

## D Introduction of the PicoScope

### D.1 Setup of the PicoScope

#### D.1.1 Hardware

Usually, the PicoScope oscilloscope can be used in the experiments without major changes to the existing experimental setup.

The power supply of the PicoScope oscilloscope is plugged in and the oscilloscope is connected to a PC via an USB cable. Four independent channels can be connected via the BNC connectors on the front. For instance, probes which are delivered with the PicoScope can simply be connected to such an input.

The used PicoScope model also features an output channel which can be adjusted with the software such that it outputs the defined function.

The described input and output connections are displayed in Figure 15.

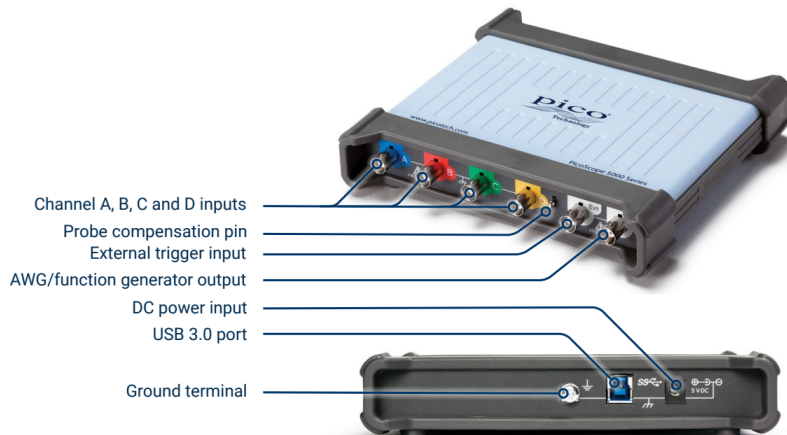


Figure 15: An overview over the inputs and outputs of a four channel PicoScope. <https://www.picotech.com/download/datasheets/picoscope-5000d-series-data-sheet.pdf>Source.

#### D.1.2 Software

On the homepage of pico Technology, the software PicoScope can be obtained which has to be installed to access and control the PicoScope oscilloscope. After starting the software, the PicoScope oscilloscope should connect automatically.

## D.2 Using the software

The basics for operating the PicoScope software are explained in this section. Also some advanced features will be described as they proved useful in the actual experiments of the lab course.

### D.2.1 General remarks

Depending on the context, it can be advantageous to save certain settings of the PicoScope in order to load them at a later time. This can be achieved at *File* → *Start-up Settings* → *Save Settings As...* and a setting file is accessed by either opening it in the Windows Explorer (if automatically associated with the PicoScope software) or use *File* → *Open*. In the menu *Start-up Settings* it is also possible to set default settings which are always loaded when starting the software or set the option to restore the settings of the last PicoScope session. The latter option is especially useful if one wants to continue with some work in the software after it was closed. Therefore, it is advised to activate this option as default settings if no user default settings are set.

### D.2.2 Scope Mode and Persistence Mode

Two different view modes are used in the lab course. The *Scope Mode* shows the signal captured during the *Collection Time* once. The *Persistence Mode* overlays multiple recorded signals and fades out the signals with time. This behaviour can be associated with the afterglow of signals on an analog oscilloscope.

Both modes share many settings regarding the display of the signal (e.g. *Input Range* and *Offset*) which are explained in Section D.2.3. However, the *Persistence Mode* features additional settings to modify the afterglow effect. Most important are the *Mode* setting (cf. Fig. 16) where *Digital Color* uses different colors to indicate how often a certain signal value occurs at a given time and *Analog Intensity* draws recent signals with full intensity while signals get paler with time. The options *Decay Time*, *Saturation* and *Decayed Intensity* define the time how long a signal takes to fade out, the intensity with which a new signal is drawn and the intensity at which signals remain after the decay time elapsed, respectively.

A special characteristic of the *Scope Mode* is the possibility to save waveforms not only as an image but also the data points in a csv or txt file. This is emphasized in Section D.2.5 and not possible in the *Persistence Mode*. It is also possible to view some previously captured signals which are stored in the buffer. Another view mode is the *Spectrum Mode* which uses a fast Fourier Transformation to display a spectrum view. As this mode is not used in the lab course currently, this feature is not covered here in further detail but information can be found in the PicoScope user's guide. Both view modes are shown in Figure 16.

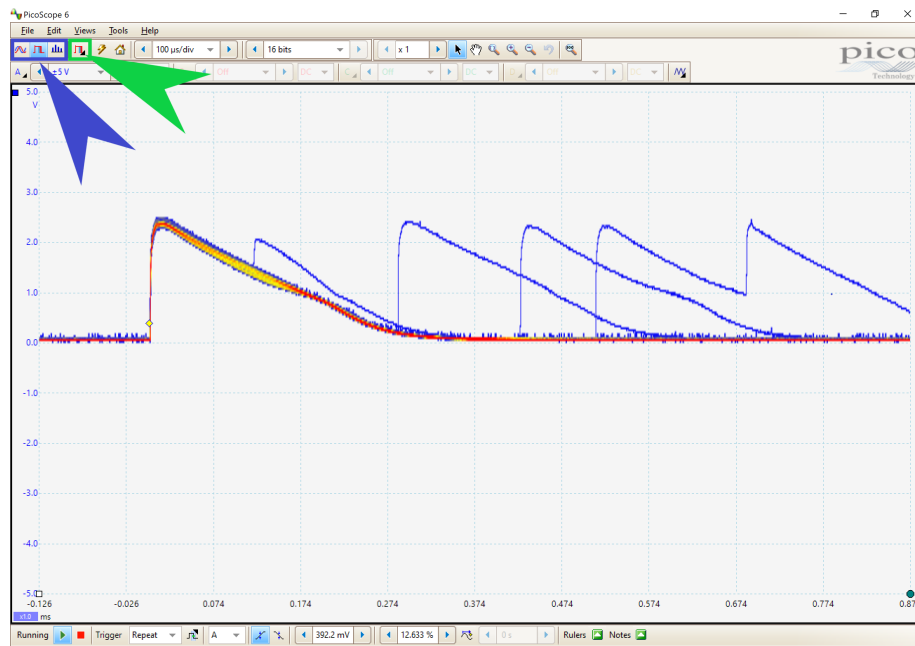
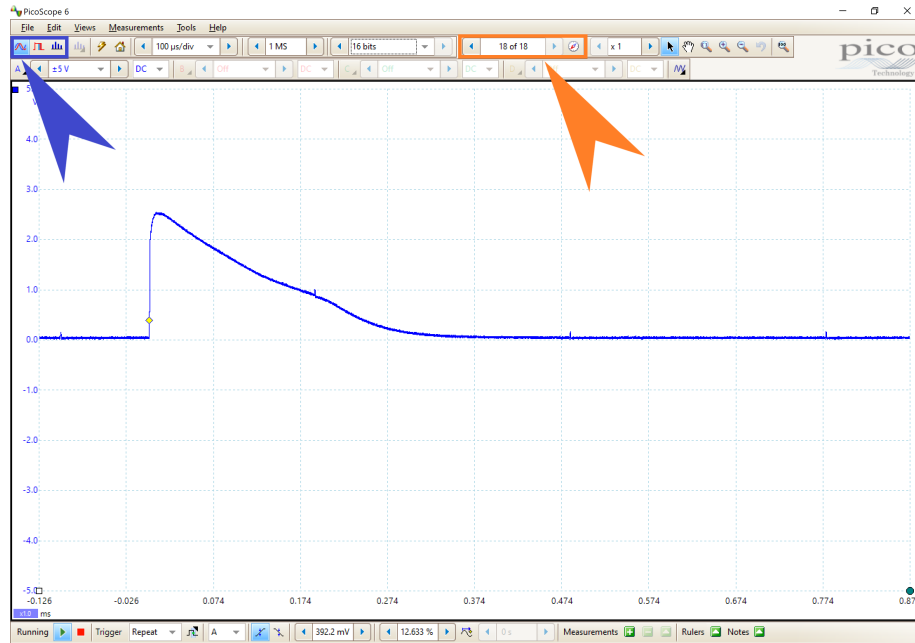


Figure 16: Displaying the signal in the *Scope Mode* (top) and *Persistence Mode* (bottom). The blue arrows indicate where the view modes can be accessed. The orange arrow shows the menu for the buffered waveforms and the green arrow marks the options for the *Persistence Mode*. A trigger has been in both view modes.

### D.2.3 Changing the display of the input signal

The different options to modify the display of the signal are explained using Figure 17. The green boxes show the options which apply to all channels.

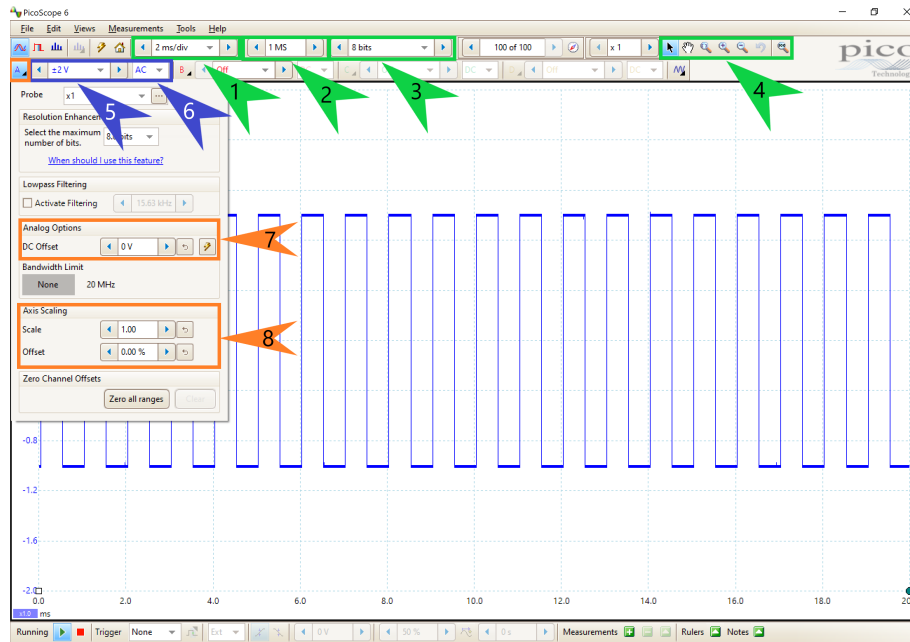


Figure 17: Options to modify the display of signals. The *Scope Mode* is used. Further information can be found in the text.

[noitemsep]The *Collection Time* determines how long a capture of a signal lasts. Usually, the time is stated per division . The total time is derived by using a factor 10 for the number of divisions. The *Number of Samples* does only need attention in some cases. The number stated is an approximate value. In the menu *Views* → *View Properties*, the actual number of samples as well as the sampling interval can be seen. For many purposes the default set value of *Number of Samples* is sufficient but for short-lived peaks and large *Collection Times* the sample interval should be considered eventually. The *Hardware Resolution* can take values from 8 to 16 bits and determines the quality of the digitized signal. Note that 15 bits and 16 bits resolution are only possible if two and one channel, respectively, are used. Using the option *Auto resolution* is usually sufficient. The zoom functions can be used to enlarge a region of the scope and investigate the waveform closer without changing the *Input Range* or *Collection Time*.

The following options can be adjusted for each channel individually.

[noitemsep]The *Input Range* option determines the minimal and maximal input value for the channel. A channel can also be turned off. If the recorded signal is larger than the *Input Range*, a warning (Channel overrange) is displayed in the upper left corner and the input range should be increased. The *Coupling* can be set to AC or DC. In the AC mode, frequencies  $\lesssim 1$  Hz are filtered out. Therefore, DC offsets are not visible,

allowing for more precise signal measurements but relative voltages with respect to the ground cannot be measured. In the DC mode, the signal is measured with respect to the ground. An *Analog Offset* can be applied to the input before digitization. This is useful cases where the maximum amplitude is known, e.g. if pulses with height 10 V are expected, the *Input Range* of  $\pm 10$  V does not have to be used but  $\pm 5$  V with an *Analog Offset* of  $-5$  V. The *Axis Scaling* options can be used to manipulate the display of the signal. In contrast to the *Analog Offset*, these options apply to the axis not the signal.

#### D.2.4 Trigger

A plethora of triggers is available which are especially useful for finding rare and short-lived signals. The options are explained with Figure 18. All options regarding trigger are set in the menu bar at the bottom of the software.

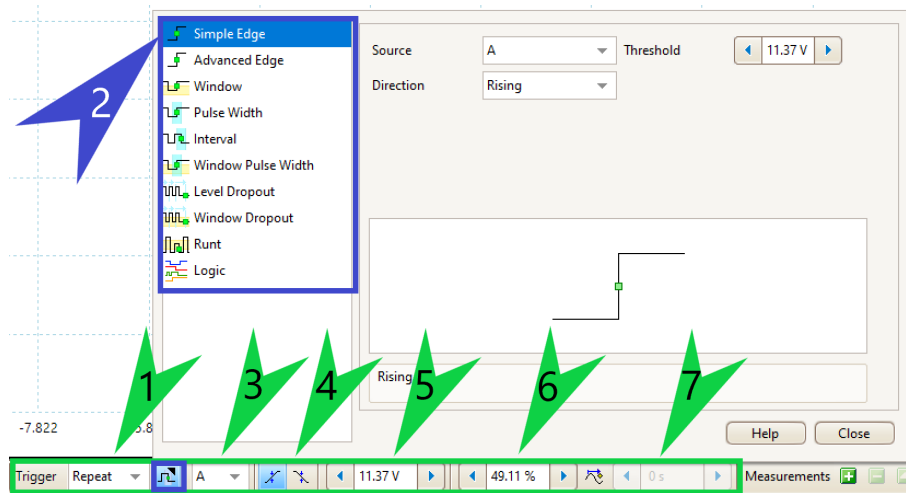


Figure 18: Trigger menu (green) at the bottom of the PicoScope menu. The context menu of the *Advanced Triggers* (blue) is shown. Further information can be found in the text.

[noitemsep]Different *Trigger Modes* are available determining what signals are displayed. The most important are

- (1) – *None*: No trigger is used.
  - *Auto*: Displays a triggered waveform but if no present the input signal is displayed regardless of the trigger.
  - *Repeat*: Displays only triggered waveforms.
- (2) *Advanced Triggers* can be used but usually the *Simple Edge* trigger is sufficient which fires when the signal passes through a certain threshold. The other triggers have additional features, e.g. allowed voltage windows for the signal. The options (3)-(5) can also be adjusted in this context menu.

- (3) Usually, the *Trigger Channel* is the same as the displayed signal. If multiple inputs are displayed, one channel has to be chosen which triggers for all inputs. It is also possible to trigger on an external channel.
- (4) The *Edge Select* option allows to trigger on either falling or rising edges.
- (5) The *Threshold* can be typed in at the menu bar, in the *Advanced Triggers* menu or by dragging the marker (yellow square in the scope) at the desired position.
- (6) The *Pre-trigger* determines how much of the signal is captured and displayed before the trigger fires. It can also be adjusted by dragging the marker in the scope.
- (7) The *Trigger-delay* has to be enabled by clicking on the respective item in the menu bar and determines how much time has to elapse before the trigger can fire again.

For most purposes, the *Simple Edge* trigger with a sufficient *Threshold* and *Pre-trigger* and correct *Edge Select* is sufficient.

### D.2.5 Saving waveforms

The PicoScope software features the saving of captured waveforms either as an image or a csv/txt file if the *Scope Mode* is used. The latter file types store single data points and are useful to analyze the waveforms with another software.

Saving a waveform can be accessed via *File* → *Save* or *Save As*. The appearing window allows to select a file location and filename for the file. Different file formats such as files readable by the PicoScope software (e.g. pssettings and psdata), text files (e.g. txt and csv) and images (e.g. png and jpg) can be chosen. The options in the window allow to save only the currently displayed waveform, all waveforms in the buffer or a subset of the buffered waveforms. If not using a PicoScope file type, a separate folder will be created if multiple waveforms are saved.

The PicoScope also allows to save the waveform automatically every time the trigger fires. For saving waveforms when the trigger fires, an alarm has to be set up in the menu *Tools* → *Alarms*. In the *Alarms* dialog window, the event has to be set to *Capture* and the first item (usually it has the name *Beep*) of the list has to be selected and edited. The action is changed to *Save Current Buffer* and a directory in which the files are saved has to be chosen. It is important to set the file type explicit to a csv-file if one wants access the data points and not only obtain an image of the waveform. The stated filename will be used for all files and numbered serially. E.g. the filename is set to be *waveform*. Then the first file is *waveform.csv*, the second is *waveform (2).csv*, the third is *waveform (3).csv* etc. The set up of the alarm is finalized by closing all dialogs with the *Save* (German: *Speichern*) or *OK* button. When starting the capturing of signals in the PicoScope software (green triangle in lower left corner), every time the trigger fires, the currently displayed waveform is stored as csv-file. To turn off the saving of pulses, it is easiest to stop the signal capture (red square in the lower left corner) and turn of the alarm in the alarm dialog window. The whole process is described in Figure 19.

## D.2.6 Measurements

The PicoScope allows to infer several values of the captured signals. These measurements can be used to count falling or rising edges which is useful in many experiments of the lab course whenever peaks are counted. Therefore, this introduction focuses on this measurement but counting peaks is not the only measurement featured by the PicoScope software.

A measurement is set up (c.f. Fig. 20) via *Measurements* → *Add Measurement* (1a) or by clicking on the + on the lower menu bar (1b). In the appearing context window, multiple settings have to be set. The input channel is assigned (2). Multiple measurements of different quantities for different channels are possible. The type of measurements is defined (3) which is *Falling Edge Count* or *Rising Edge Count* if the number of peaks is supposed to be measured. It is possible to use the whole trace for a measurement or only a latter defined interval  $\Delta t$  (4). The measurement options allow either a threshold to be defined or an automatic threshold to be used (5). The hysteresis can be leaved unchanged. This parameter is linked to a mechanism that prevents wrongly counts due to fluctuations of the signal near the threshold. More information on that are provided in the PicoScope user's manual. If the options to use the whole trace and an automatic threshold, the measurement is ready to start. Otherwise, the rulers on the horizontal and vertical axis have to be adjusted to determine the measurement range and the threshold, respectively (c.f. Fig. 21). The values can either be typed in the ruler legend or defined by dragging the rulers to the desired position. The measurement is found at the bottom with multiple values shown.

[noitemsep]The used *Channel* and *Measurement mode* are shown. The *Value* refers to the counted edges in the currently displayed waveform. The values *Min* and *Max* show the minimum and maximum counted edges, respectively, in a waveform. The *Average* is defined by the arithmetic average of the counts in the waveforms. The standard deviation  $\sigma$  is defined by  $\sigma^2 = \frac{1}{N-1} \sum_{i=1}^N (y_i - \bar{y})^2$  where  $N$  is the number of captured samples,  $y_i$  the number of edges in the  $i$ -th sample and  $\bar{y}$  the mean of counted edges over all samples. The *Capture Count* determines how many captured samples are considered. More samples result in better statistics but need more time to be collected. In case the number of captured samples exceeds the *Capture Count*, every new samples replaces the oldest considered sample. Consequently, the other values such as *Min* and *Max* only refer to the currently considered samples and not to all samples ever captured. The *Capture Count* can be changed at *Tools* → *Preferences* → *General* → *Measurement Statistics*. The *Span* shows if a ruler-defined  $\Delta t$  is used or the whole trace.

In Section ?? a description is provided on how to access the measured values automatically. Note that a measurement can fail which is displayed by - - in the overview of the measurement results. This problem can usually be solved by either decreasing the *Collection Time* or by reducing the *Number of Samples*. Which solution is better depends on the context of the measurement but if using the latter solution one should check that the sampling interval is still large enough to capture the signals.

**Note:** When using large *Collection Times* ( $\geq 100$  ms/div), the PicoScope has to be hindered to go into the *Slow Sampling Mode* otherwise wrong measurement results are obtained. This is achieved at *Tools* → *Preferences* → *Sampling* → *Slow Sampling Transition*. Here, a *Collection Time* larger than the one used in the measurement has to be chosen.

### D.2.7 *Math Channel*

The PicoScope software features *Math Channels* which allow to manipulate one or multiple inputs with mathematical expressions. The output is displayed as an additional waveform in the scope and can also be used as an input channel for measurements.

*Math Channels* are accessed via *Tools* → *Math Channels*. The featured built-in operations are inverting the signal, adding, subtracting, multiplying and dividing two signals. It is also possible to define functions by clicking on *Create* in the *Math Channel* menu and entering the desired expression.

An application of *Math Channels* is the implementation of a coincidence counter. Two input channels which are assumed to be 0 V by default, i.e. in the digital LOW state, and have a non-zero voltage if they are in the digital HIGH state are multiplied. Only if both channel are in the digital HIGH state, the function has a non-zero output which is an implemented logical OR gate. In order to count the number of coinciding events, a measurement counting the rising or falling edges of the function can be used.

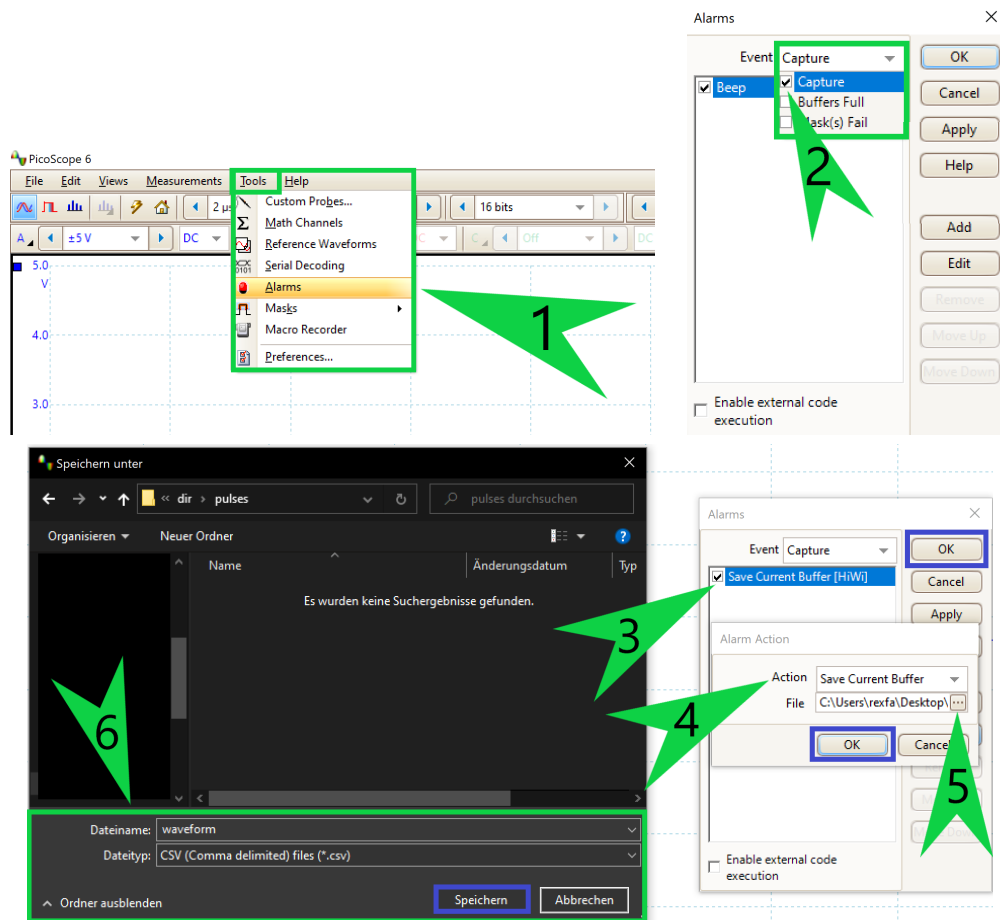


Figure 19: Saving pulses on trigger. In the *Alarm* dialog window (1), *Capture* has to be selected as event by checking the tick box (2). A new dialog window is opened (lower image) by editing the item in the list (3). The action is set to *Save Current Buffer* (4) and the directory, filename and file type are specified (5, 6) in the next dialog window. The file type should be set to csv if the data is analysed with another software afterwards. At last, all windows are closed (blue boxes).

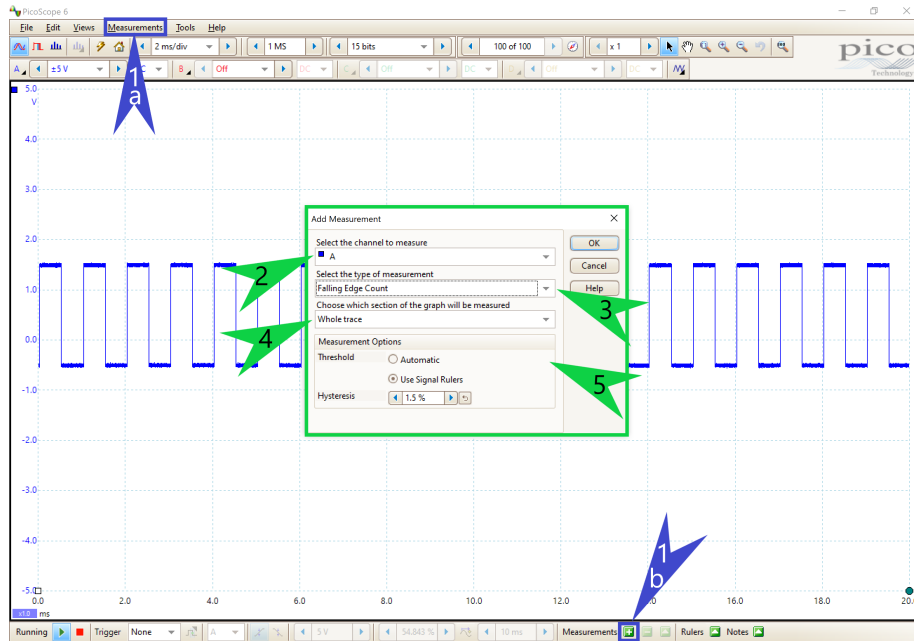


Figure 20: The measurement window (green frame) is opened via the menus indicated by the blue arrows. Further information can be found in the text.

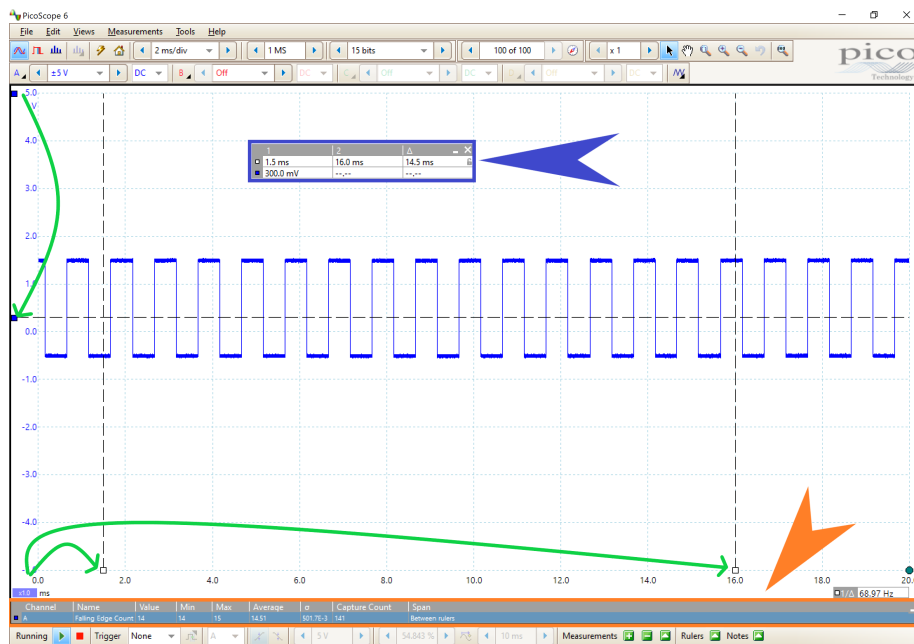


Figure 21: Finalizing the measurement by adjusting the ruler (green arrows) or using the ruler legend (blue arrow). The measurement results are displayed at the bottom (orange arrow). Further information can be found in the text.